AD-783 200

EXPERIMENTAL EVALUATION OF COATED
GRAPHITE ICBM ROCKET NOZZLE THROAT
INSERTS

Jay G. Baetz

Aerospace Corporation

Prepared for:

Space and Missile Systems Organization

12 June 1974

Approved

W. C. Riley, Director

W. C. Riley, Director
Materials Sciences Laboratory
Laboratory Operations

Publication of this report does not constitute Air Force approval of the report's findings or conclusions. It is published only for the exchange and stimulation of ideas.

Richard J. Rynearson

Richard J. Rynearson, Lt, USAF
Technology Development Division
Deputy for Technology

ib

AD 783 200

REPORT DOCUMENTATION PAGE

READ INSTRUCTIONS
BEFORE COMPLETING FORM

1. REPORT NUMBER	2. GOVT ACCESSION NO.	3. RECIPIENT'S CATALOG NUMBER
SAMSO-TR-74-158		

4. TITLE *(and Subtitle)*	5. TYPE OF REPORT & PERIOD COVERED
EXPERIMENTAL EVALUATION OF COATED GRAPHITE ICBM ROCKET NOZZLE THROAT INSERTS	Interim
	6. PERFORMING ORG. REPORT NUMBER TR-0075(5546)-1

7. AUTHOR(s)	8. CONTRACT OR GRANT NUMBER(s)
Jay G. Baetz	F04701-74-C-0075

9. PERFORMING ORGANIZATION NAME AND ADDRESS	10. PROGRAM ELEMENT, PROJECT, TASK AREA & WORK UNIT NUMBERS
The Aerospace Corporation El Segundo, Calif. 90245	

11. CONTROLLING OFFICE NAME AND ADDRESS	12. REPORT DATE
Air Force Rocket Propulsion Laboratory Air Force Systems Command Edwards, Calif. 93523	12 June 1974
	13. NUMBER OF PAGES 72

14. MONITORING AGENCY NAME & ADDRESS *(if different from Controlling Office)*	15. SECURITY CLASS. *(of this report)*
Space and Missile Systems Organization Air Force Systems Command Los Angeles, Calif. 90045	Unclassified
	15a. DECLASSIFICATION/DOWNGRADING SCHEDULE

16. DISTRIBUTION STATEMENT *(of this Report)*

Approved for public release; distribution unlimited

17. DISTRIBUTION STATEMENT *(of the abstract entered in Block 20, if different from Report)*

18. SUPPLEMENTARY NOTES

19. KEY WORDS *(Continue on reverse side if necessary and identify by block number)*

Codeposited silicon carbide and pyrolytic graphite
Degree of graphitization
Deposition parameters
Microstructure

20. ABSTRACT *(Continue on reverse side if necessary and identify by block number)*

An empirical procedure for determining the net residual stress of a typical ICBM coated nozzle throat insert is described. The experiment includes provisions for separating substrate-induced stresses from the primary and secondary coating stresses. The results of such experiments conducted on a pure pyrolytic graphite coated insert and on a codeposited silicon carbide and pyrolytic graphite insert are discussed.

DD FORM 1473
(FACSIMILE)

19. KEY WORDS (Continued)

Pyrolytic graphite coatings
Residual stresses
Rocket nozzle thermal response
Solid propellant rocket nozzles
Thermal expansion
Unit cell height

20. ABSTRACT (Continued)

In addition, the determination of thermal expansions of up to $5000°F$ is presented for various coating materials. An examination of unit cell height C_o, including experimentally determined values for both as-deposited and thermally loaded coating materials, is discussed relative to the thermal and mechanical properties of the coating. A brief discussion is presented of a process for depositing a pyrolytic graphite coating in which certain parameters are varied during the course of deposition (referred to as a mode process by the fabricator).

ia

PREFACE

CONTENTS

Preceding page blank

-3-

FIGURES

Preceding page blank

TABLES

I. INTRODUCTION

The successful performance of ICBM rocket nozzle throat inserts made of coated graphite has been impeded, in part, by the excessive stresses that exist in the coating. These stresses are primarily a result of the coupling of overall residual stresses inherent in the processing technique with thermally induced rocket motor firing stresses. Because the firing stresses are a result of fixed stimuli, they themselves are essentially fixed stresses. Therefore, if the coating stress problem is amenable to solution, the residual stresses must represent a significant portion of the total stress state. Furthermore, these stresses must be reducible.

In order to evaluate the former postulate, The Aerospace Corporation, under the direction of the Air Force Rocket Propulsion Laboratory (AFRPL), has experimentally determined the peak residual strain levels in several ICBM inserts. Strain profiles were interpolated for inside diameter coating surfaces as well as for primary coating stresses. Also, strains resulting from the interaction of the substrate and coating were separated from those of the primary and secondary coatings. Two residual stress experiments were performed during the first half year of this program. The initial experiment was conducted on a nozzle insert with an inside diameter of 13 in. and consisting of a pyrolytic graphite (PG) coating over an AGSR polycrystalline graphite substrate. The second experiment utilized a nozzle insert with an inside diameter of 12-1/2 in. and consisting of a codeposited silicon carbide and pyrolytic graphite (SiC/PG) coating on an ATJ polycrystalline graphite substrate. Both of these inserts were fabricated by Atlantic Research Corporation (ARC). The PG insert was made as part of the deposition scale-up task of Contract F04611-70-C-0009 with AFRPL. The SiC/PG codeposited insert was fabricated for the Naval Ordnance Systems Command (NOSC), who donated it for this effort.

Significant findings of these experiments have been: (1) the maximum residual stress of the codeposit insert is less than 2000 psi in tension at the

inside diameter coating, while the comparable stress level for the PG insert is over 5000 psi (5000 to 12,750 psi, depending on which material properties are to be believed) and is compressive at the inside diameter; and (2) most of the residual stresses are induced by the interaction of the substrate coating on cool down from deposition, not from stress, in the coating itself, which is opposite in direction to the substrate-induced stress. This last finding is especially significant for PG inserts, as it implies that there is a need for either a much improved coating-substrate compatibility or an uncoupling of the coating and backup.

The fact that the coefficient of thermal expansion α is critical to both the residual stress and thermal response stress of a given coating makes it vital that this property be known for each system up to the expected firing temperatures. As part of the effort for this program, curves that relate coating thermal expansions (both a-b and c directions) to temperature have been developed from room temperature to 5000°F for several graphite coatings. Key findings of this portion of the program were: (1) the PG as deposited by ARC is the most isotropic form of PG of those evaluated; (2) the PG from United Kingdom (UK) exhibited the high degree of anisotropy that is characteristic of a substrate-nucleated deposition process. In this regard it had a thermal expansion profile quite similar to the original material from the Hi-Temperature Materials Corporation (HTM); and (3) curves showing thermal expansion vs temperature for the various codeposited SiC/PG coatings matched closely those developed by the Southern Research Institute (SoRI) for ARC.

Little is currently understood about the significance of thermally induced microstructural changes in the graphite coating that result from rocket motor firings. In an attempt to initiate some understanding in this area, the third laboratory task in this program has been directed toward examining the changes in unit cell height C_o, which is a key, thermally sensitive, material characteristic. Perhaps the most important finding in this area to date has

been the extreme sensitivity of unit cell height to the interactions of both temperature and time.

A more detailed account of the specific laboratory experiments is presented in the sections that follow. Also presented are the conclusions that were drawn from the experiments and the recommendations for additional effort.

II. PROCEDURES AND RESULTS

A. RESIDUAL STRESSES

During this reporting period, two residual stress experiments were conducted. The initial experiment utilized a nozzle throat insert with an inside diameter of 13 in. and with a PG coating over an AGSR graphite substrate. This nozzle insert was fabricated for AFRPL by ARC as a part of the deposition scale-up task of Contract F04611-70-C-0009, "Development of Large-Diameter, High Chamber Pressure, Throat Insert Material." The second experiment was conducted on a nozzle throat insert with a nominal inside diameter of 12-1/2 in. and with a codeposited SiC/PG coating over an ATJ substrate. This insert, code No. 001-51, was fabricated by ARC under Contract N00017-73-C-4312 to NOSC. Both inserts were representative of the lower-stage designs of the ICBM.

The objectives of this study were: (1) to determine the magnitude and direction (tensile or compressive) of the circumferential and axial residual strains in the nozzle inserts at the surface of each coating; (2) to separate and define those strains induced by the substrate-coating interaction during cool down from deposition temperature; (3) to establish the bounds, or end-points, of the inner and outer coating strains; (4) to determine, in so far as material properties are available and within the validity limits of the basic equation to the complex nozzle shape, the stresses for the measured strain values; and (5) to compare the resultant stress with the analytically predicted maximum stress and with the appropriate measured stress-strain curves.

1. PYROLYTIC GRAPHITE INSERT

The PG coated nozzle insert was instrumented with 24 surface strain gages — 20 (single) BAE-13-125BB-120 gages and 4 (biaxial) EA-06-125TM-120 gages. Eastman 910 was used as the strain gage adhesive. The positioning of the gages on the surface of the PG coating and on the exit surface of the AGSR substrate is shown in Figs. 1 and 2. A full bridge was used to
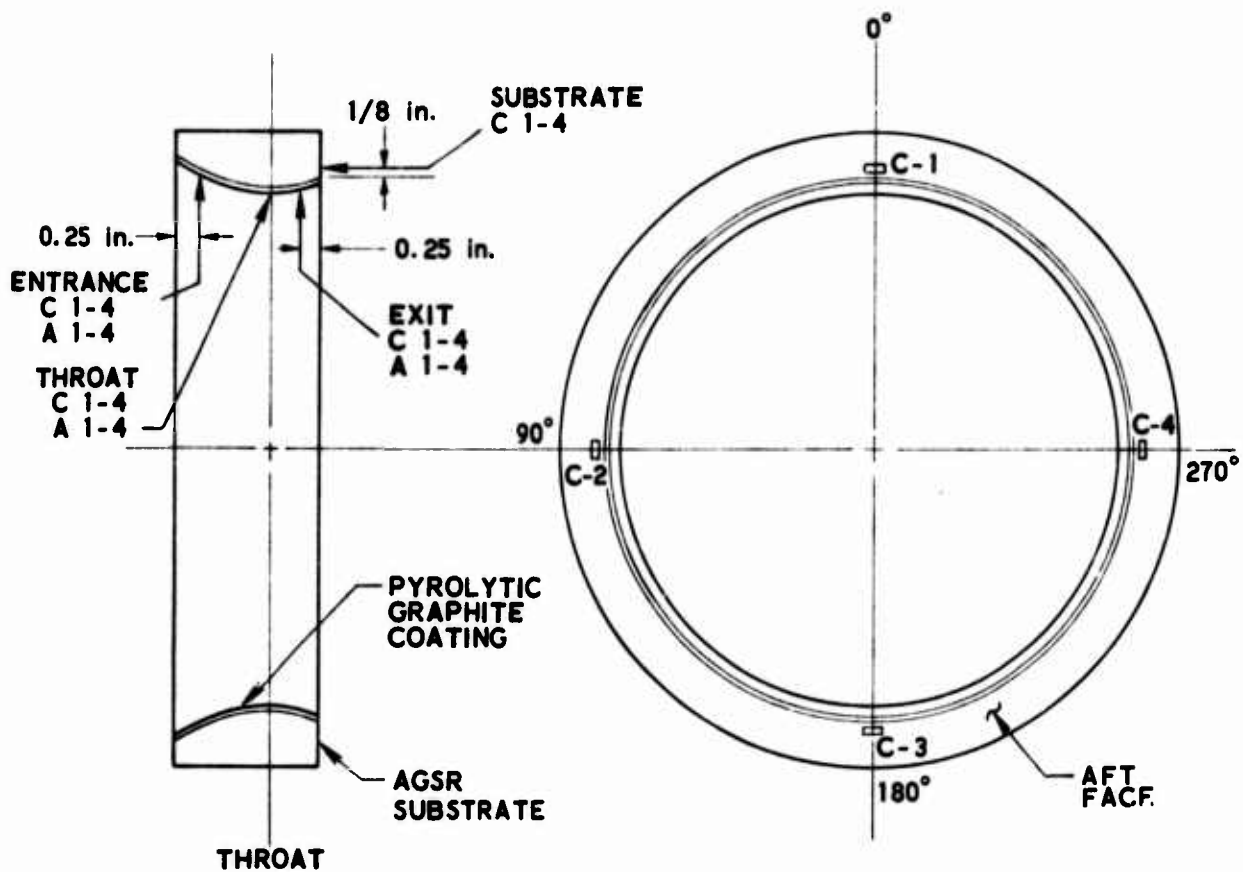
Fig. 1. Top and Section Views of Throat Insert for a Pyrolytic Graphite Coated Nozzle Showing Strain Gage Positions
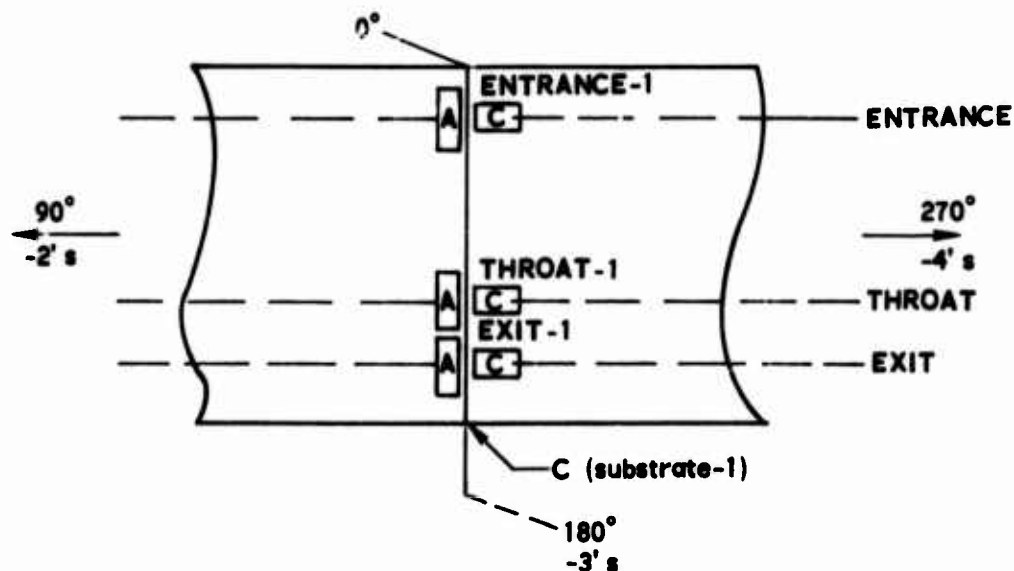
Fig. 2. Front View of Throat Insert for a Pyrolytic Graphite
Coated Nozzle Showing Strain Gage Positions

minimize the temperature effects for each reading, i.e., one active gage
on the 13-in. inside diameter, PG-coated nozzle insert and three dummy
gages on a 7-in. inside diameter, PG-coated nozzle insert.

A Vishay high-sensitivity, digital strain indicator with internal cali-
bration, Model V/E-120, was used to measure the strain output. A 36-
position switching box was also designed to minimize contact resistance
by (1) employing a three-point contact at each position of the nonshorting
rotary switches and (2) soldering the leads from the strain gages directly
to the switches. This eliminated the use of banana plugs and jack
connectors.

The axial planar locations of the strain gages were as follows:

a.   The entrance gages are 0.25 in. in from the forward edge on
       the PG coating.

b. The throat gages are at the minor inside diameter of the PG coating.

c. The exit gages are 0.25 in. in from the aft edge of the PG coating.

d. The substrate gages are on the aft face of the AGSR substrate and are 1/8 in. outward from the inside edge of the PG coating.

The circumferential locations of the strain gages were as follows:

a. For all axial coating planes, the axial (A) and circumferential (C) gages are numbered 1 through 4 counterclockwise at 90-deg increments. The axial gages are to the left of each quadrant marker, and the circumferential gages are to the right (see Fig. 2).

b. The substrate gages are the same as the PG coating except that only circumferential gages were used.

The following procedures were performed:

a. Strain readings were taken from each gage.

b. The nozzle insert was clamped into the fixture and placed into the lathe.

c. 0.050 in. was removed from the outside of the AGSR substrate.

d. The nozzle insert and fixture were removed from the lathe and unclamped.

e. Strain readings were then taken.

This cycle was repeated until fracture of the nozzle insert occurred. The procedures followed in this experiment are shown in Figs. 3 through 11. Partial failure of the insert proved somewhat unfortunate as it precluded the development of any strain profile through the thickness of the coating. It also clouded a precise separation of the substrate-induced stresses from the coating stresses. Failure appeared to initiate at the outside diameter of the reduced substrate and propogate through the AGSR to the PG interface and on into the PG itself. It is postulated that the crack continued into the PG by cleaving the disordered a-b planes and extended further into the PG until a major delamination acted as a "crack stopper." The appearance of the failure at this point is shown in Fig. 12.

The circumferential and axial strain data are presented in Figs. 13 through 18. Readings were taken at θ = 0, 90, 180, and 270 deg, and the curves represent average values. After fracture occurred, a grinding operation was employed to totally remove the AGSR substrate. Final readings were taken, and these are indicated on each figure. It is unfortunate that the failure described above occurred, as it masked the attempt to separate the substrate-induced stresses from the coating deposition stresses. It also prevented the observation of the anticipated reversal of the hoop stress that was expected at a substrate reduction of about 90 percent. The dotted median lines of Fig. 13 illustrate the conjectured response. The hypothesis is based on the fact that the inner surface of the integral coating-substrate exhibits a compressive strain condition whereas the inner surface of the coating by itself (free-standing) should exhibit a tensile strain as a result of the primary and secondary stress-inducing conditions of deposition. This point is graphically illustrated in Fig. 19, which shows a rather undesirable way of relieving the inside diameter tensile loading and outside diameter compressive loading of a PG throat insert.

The plots of strain values vs the percent of substrate removed do illustrate the fact that the highest level of both circumferential and axial strains at the inside diameter coating occur near the exit plane, and that the circumferential strains are significantly greater in magnitude than the axial strains. Furthermore, an examination of the extrapolated data spread indicates a relatively low order of pure coating strains. Whatever the magnitude of these strains, they are, if anything, a help to the overall stress picture, because both the substrate-induced strains and the thermal strains encountered in firing are hightly compressive and additive at the coating surface. The direction of the maximum surface strains and stress reversals of the coating-substrate composite to the surface stresses of the free-standing coating are in agreement with the early efforts of Lozier and Manobsky (Ref. 1), and by HTM (Ref. 2).

Up to this point, all specific references to the numerical results of this experiment have been to strain values. This has been done primarily because of the low confidence level in the material property inputs to the basic stress-strain equation. There also must be a question of the applicability of the equation to such a highly anisotropic material of such complex shape. (Shape effects, if any, will be examined in subsequent work by comparisons of nozzle insert data to simple cylinders.) The stress data discussed in the paragraphs that follow should therefore be tempered with this input.

Stress-strain variations of Hooke's law for isotropic materials can be used to determine the stress directly from the strain if the following is assumed:

a.   Radial stress is zero.

b.   Poisson's ratio ν and elastic modulus E are constant and independent of circumferential and longitudinal stresses.

c.   Strains are in principal directions.

By means of these assumptions, the following equations were derived:

$$\sigma_c = \frac{E}{1 - \nu^2} (e_c + \nu e_1) \tag{1}$$

$$\sigma_1 = \frac{E}{1 - \nu^2} (e_1 + \nu e_c) \tag{2}$$

where

σ_c = circumferential stress

σ_1 = longitudinal or axial stress

e_c = circumferential strain

e_1 = longitudinal or axial strain

The location of the defined stress components are shown in Fig. 20.
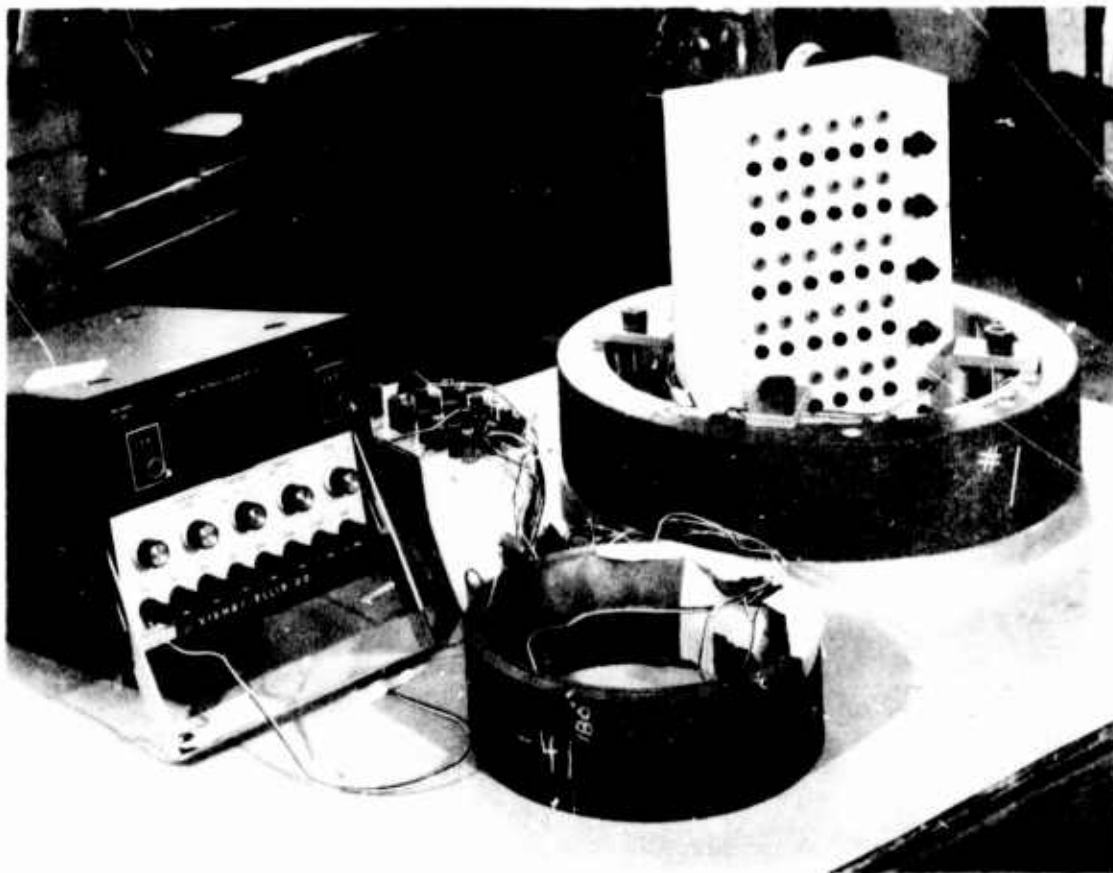
Fig. 3. Experimental Setup Used for Stabilization
Studies Prior to Dissection

Fig. 4. AGSR Substrate Shown on Lathe Prior to
Cutting Operation
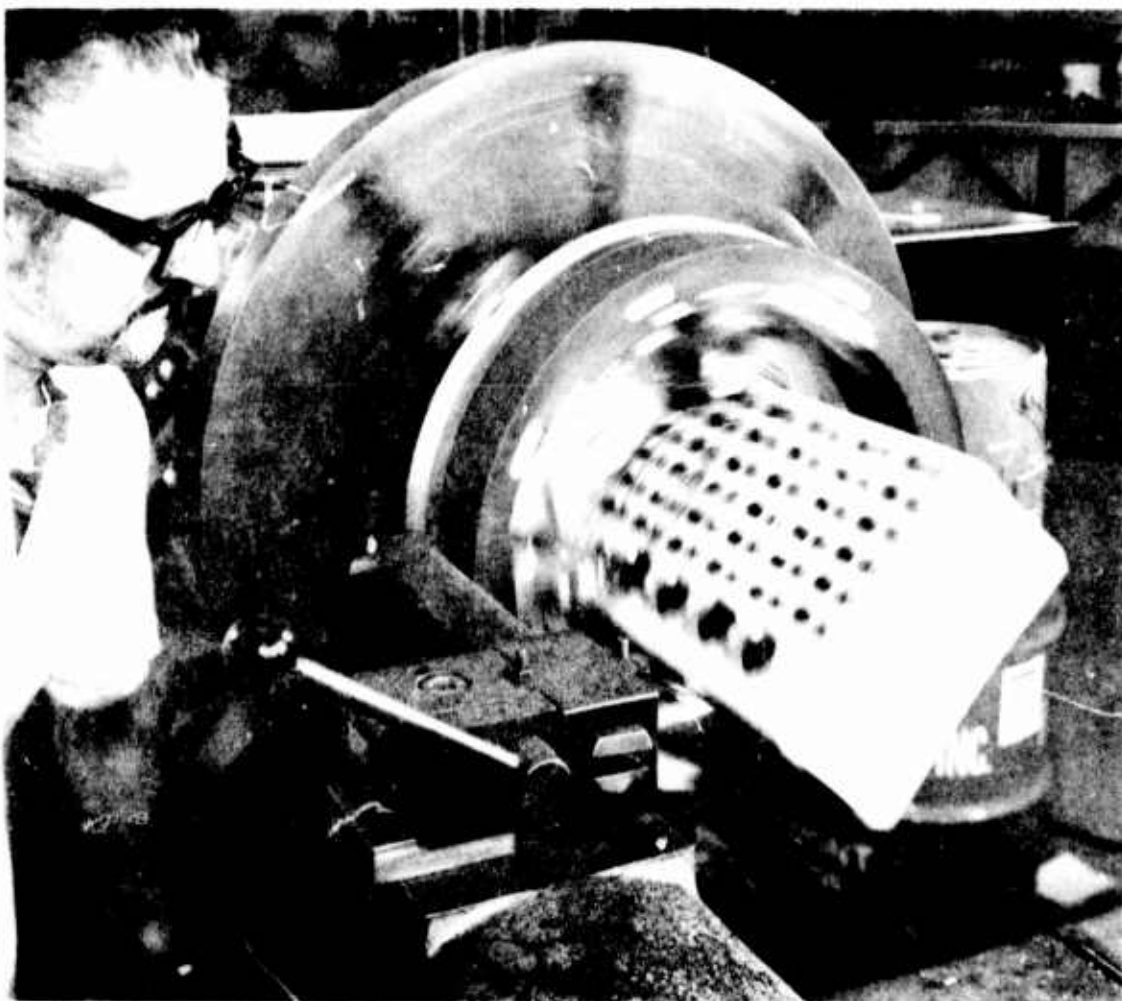
Fig. 5. AGSR Substrate Removed by Lathing Operation
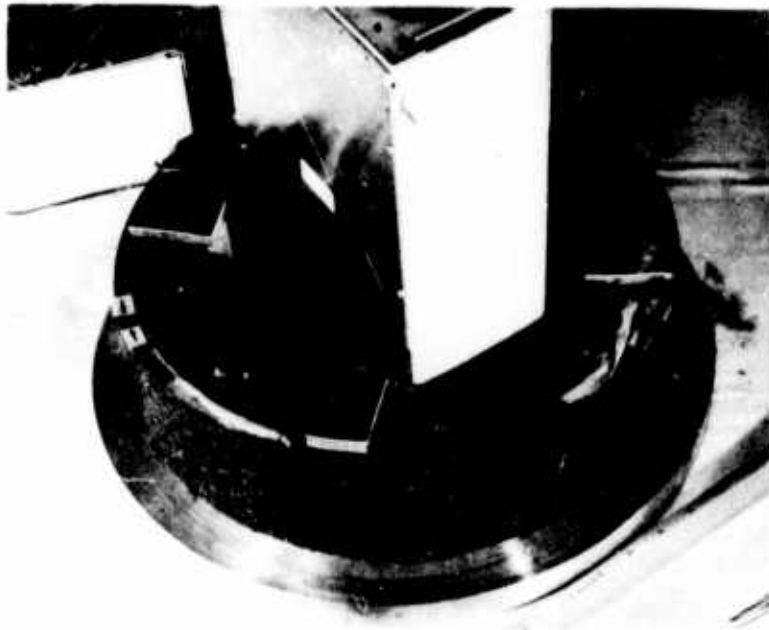
Fig. 6. Position of Two Cracks that Occurred
After Removal of 1.10 in. of Substrate
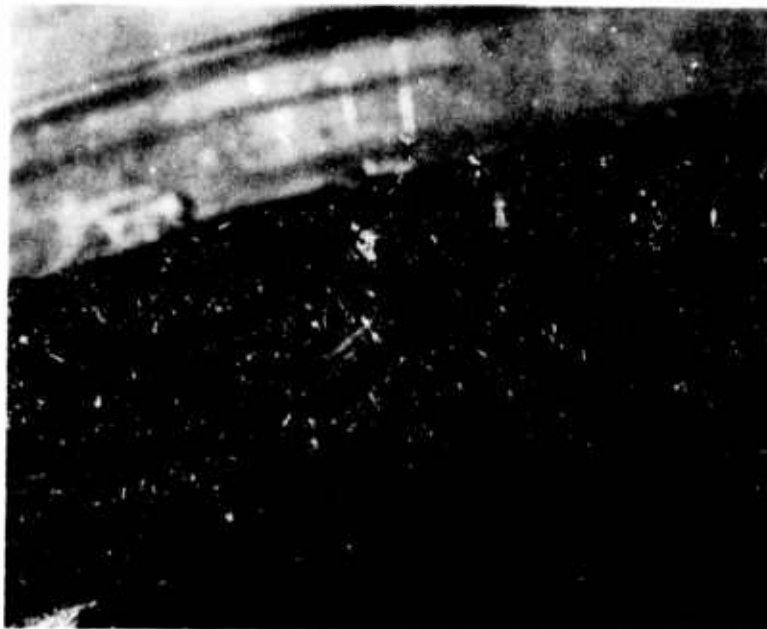
Fig. 7. Closeup of Crack from Top Showing
Delamination of PG Coating
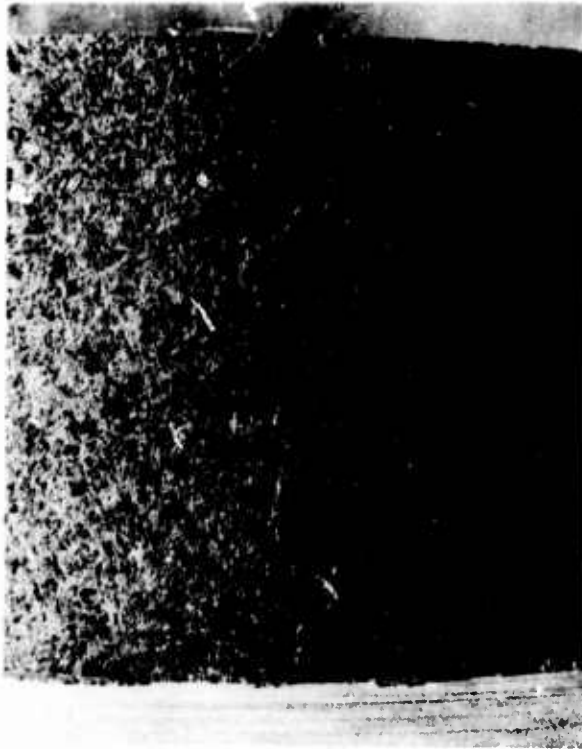
Fig. 8. Outside Surface
Fracture of
AGSR Substrate

Fig. 9. Closeup of Frac-
ture Surface of
PG Coating Show-
ing Laminar
Nature of Fracture
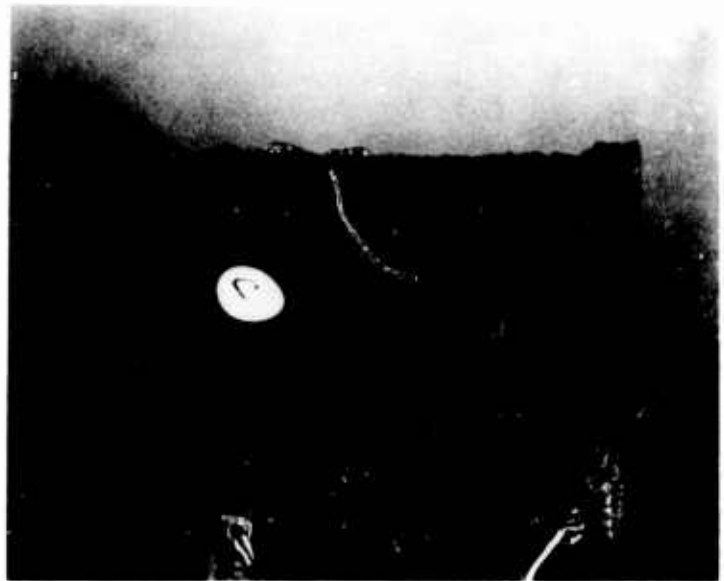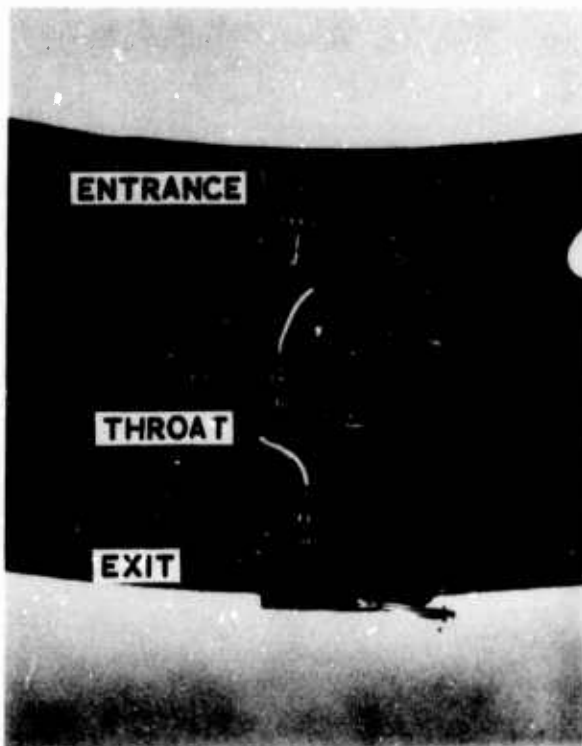
Fig. 10. Orientation of Strain Gages on Surface of PG Coating

Fig. 11. PG Coating with AGSR Substrate Completely Removed and After Slitting
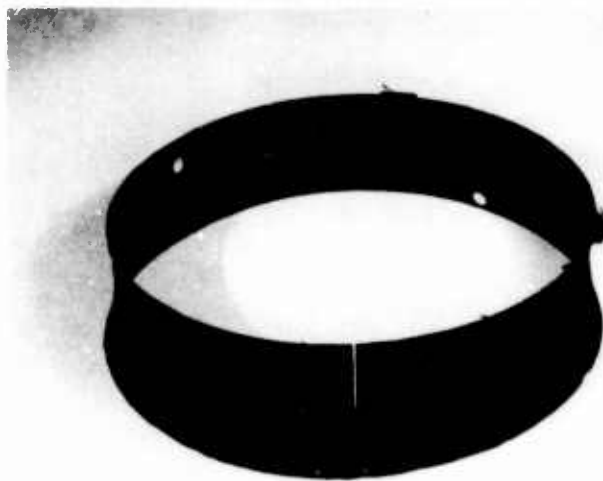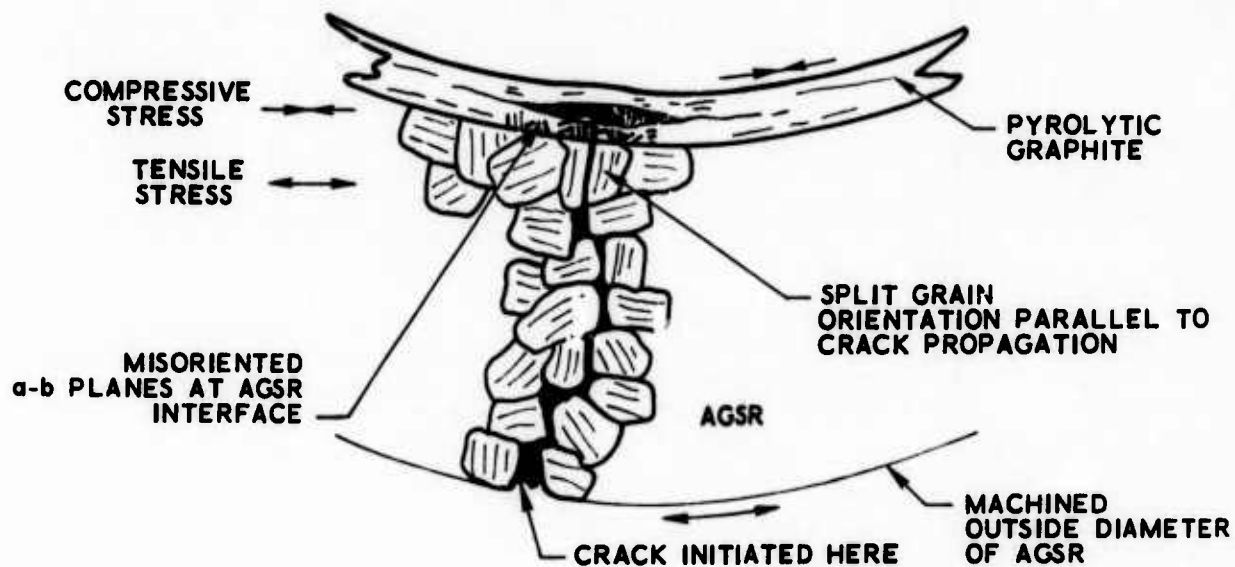
Fig. 12. Schematic of Insert Failure Region

ab STRAIN RELIEF AS A RESULT OF SUBSTRATE LATHING
bc EXTRAPOLATED STRAIN RELIEF AFTER NOZZLE FRACTURED
cd APPARENT STRAIN RELIEF OF PYROLYTIC GRAPHITE SHELL
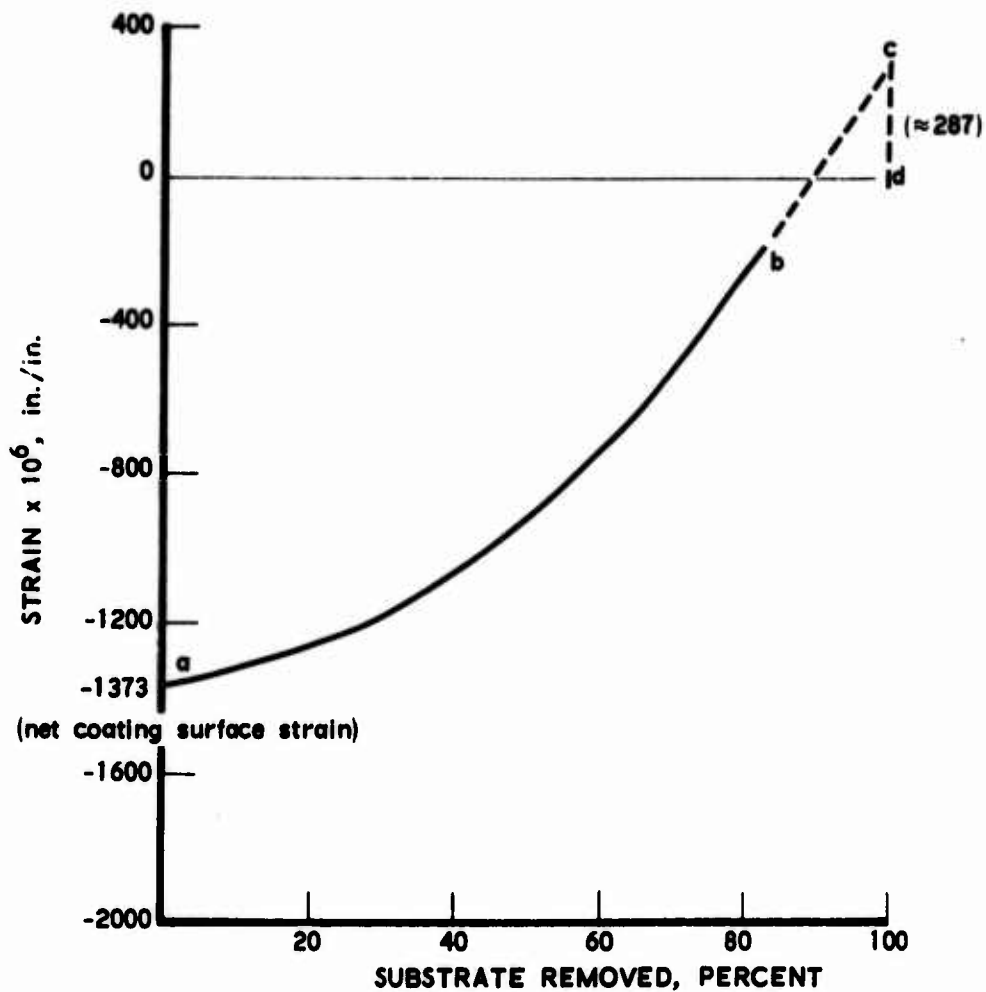
Fig. 13. Circumferential Strain Relief of PG
Coating Surface at Entrance

ab STRAIN RELIEF AS A RESULT OF SUBSTRATE LATHING
bc EXTRAPOLATED STRAIN RELIEF AFTER NOZZLE FRACTURE
cd APPARENT STRAIN RELIEF OF PYROLYTIC GRAPHITE SHELL
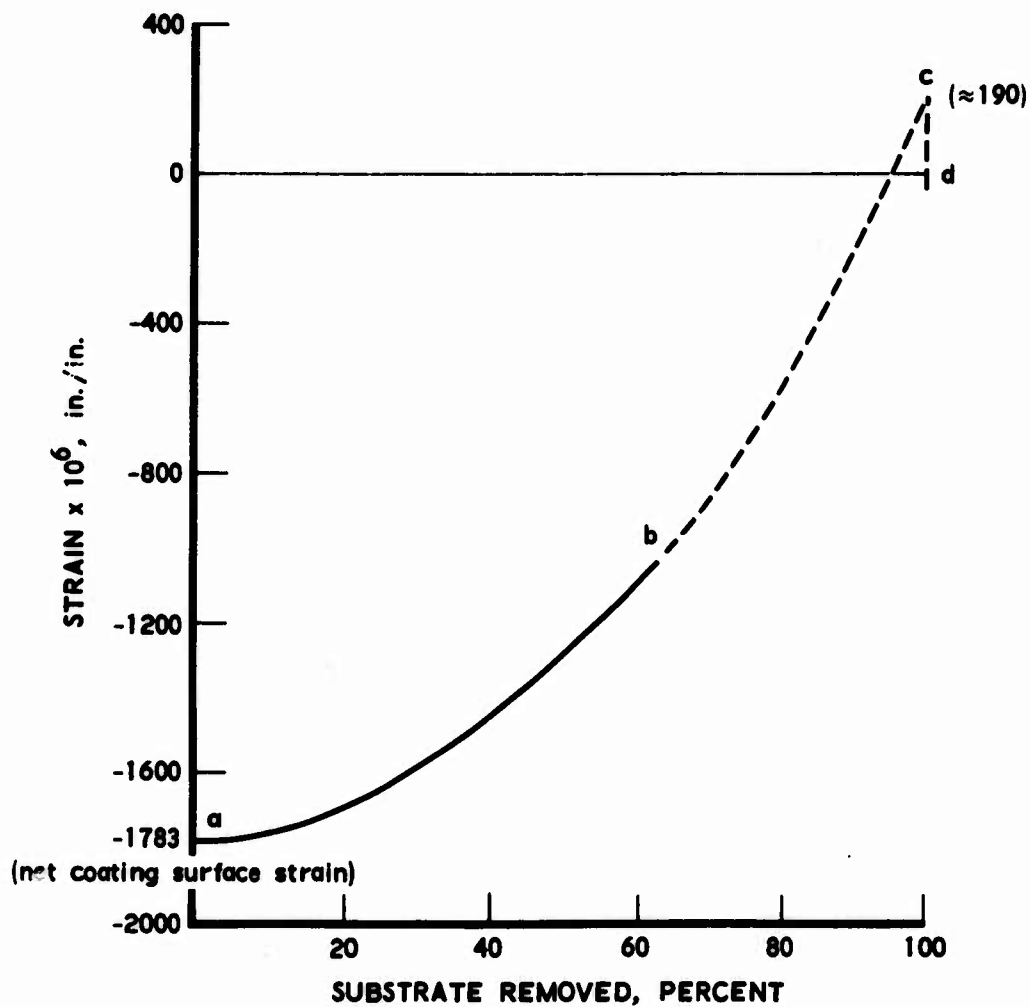
Fig. 14. Circumferential Strain Relief of PG
Coating Surface at Throat

ab STRAIN RELIEF AS A RESULT OF SUBSTRATE LATHING
bc EXTRAPOLATED STRAIN RELIEF AFTER NOZZLE FRACTURE
cd APPARENT STRAIN RELIEF OF PYROLYTIC GRAPHITE SHELL

Fig. 15.   Circumferential Strain Relief of PG
Coating Surface at Exit

ab STRAIN RELIEF AS A RESULT OF SUBSTRATE LATHING
bc EXTRAPOLATED STRAIN RELIEF AFTER NOZZLE FRACTURE
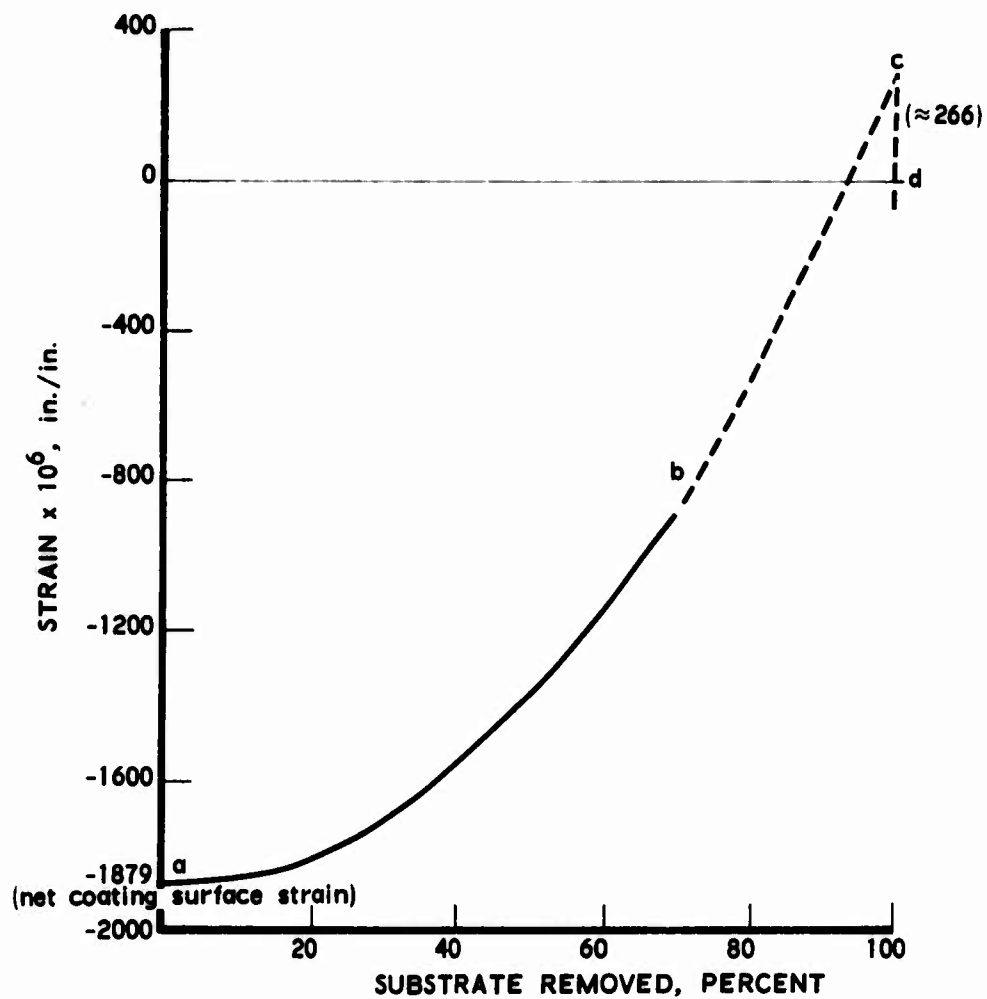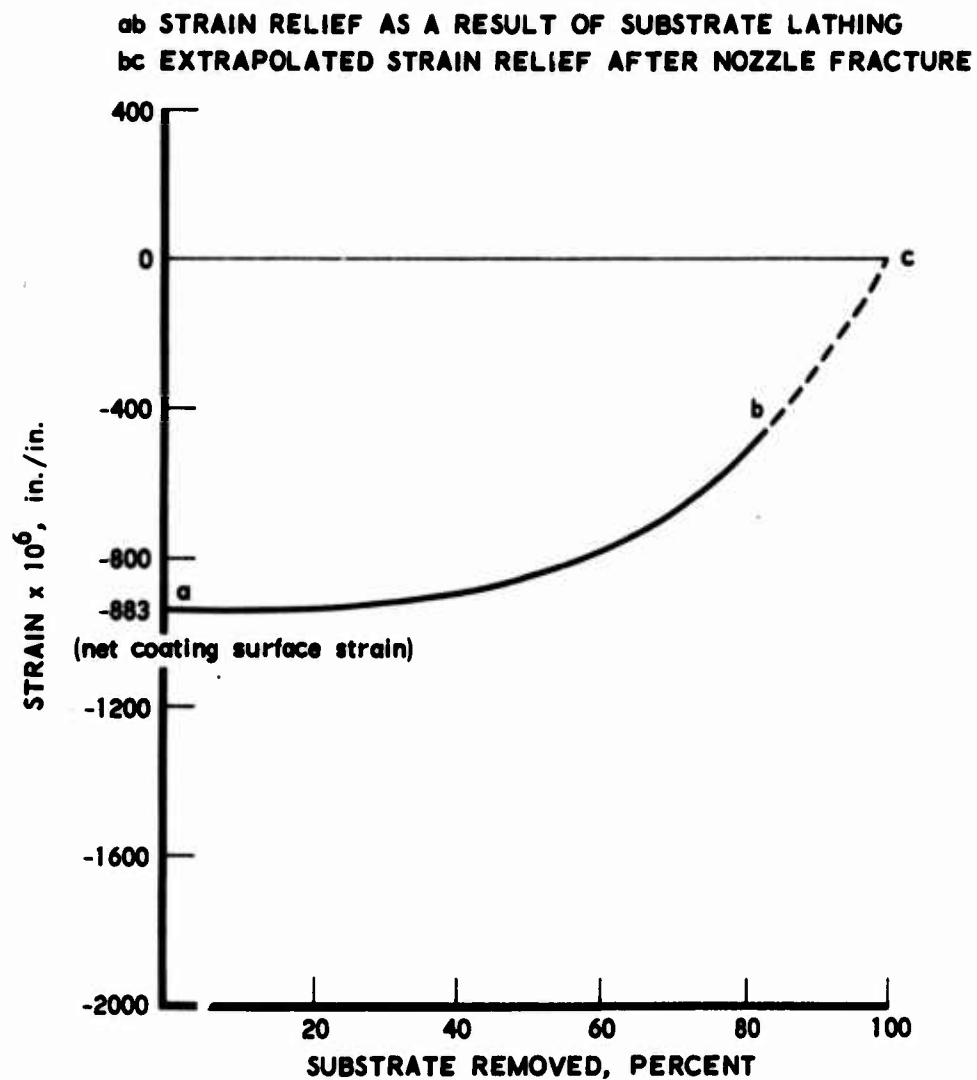
Fig. 16.   Axial Strain Relief of PG Coating
Surface at Entrance

ab STRAIN RELIEF AS A RESULT OF SUBSTRATE LATHING
bc EXTRAPOLATED STRAIN RELIEF AFTER NOZZLE FRACTURE
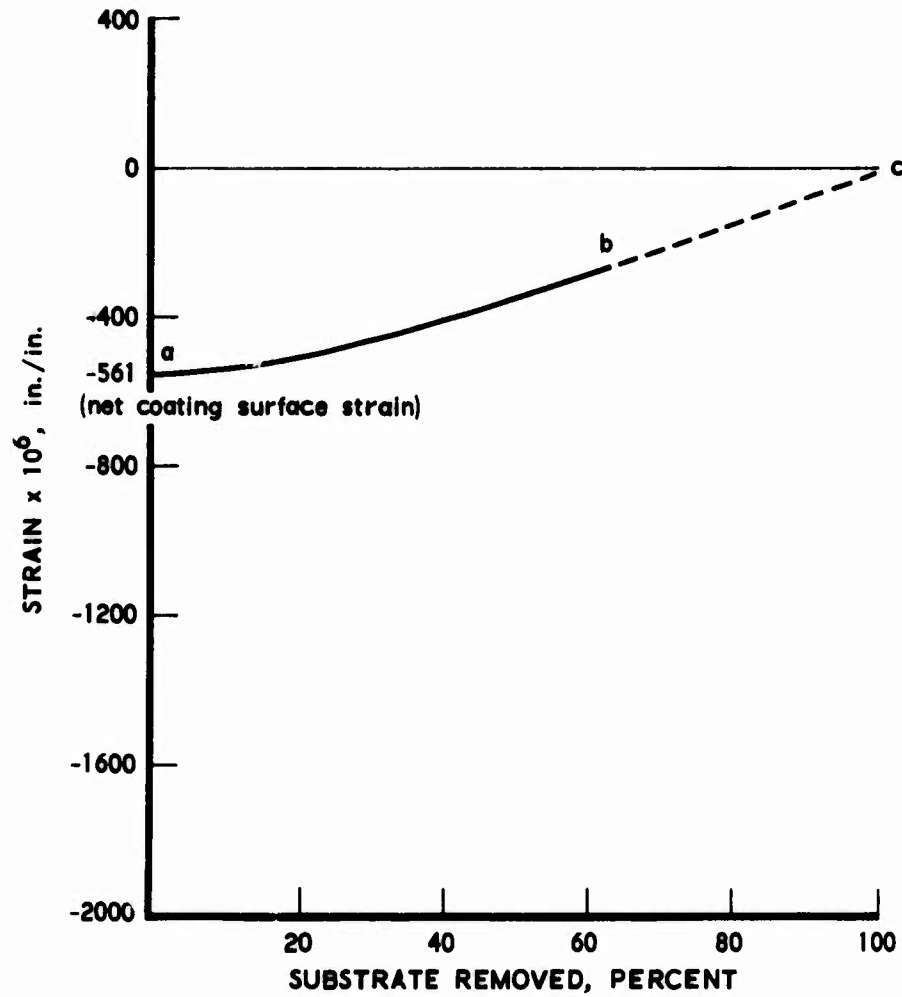
Fig. 17. Axial Strain Relief of PG Coating
Surface at Throat
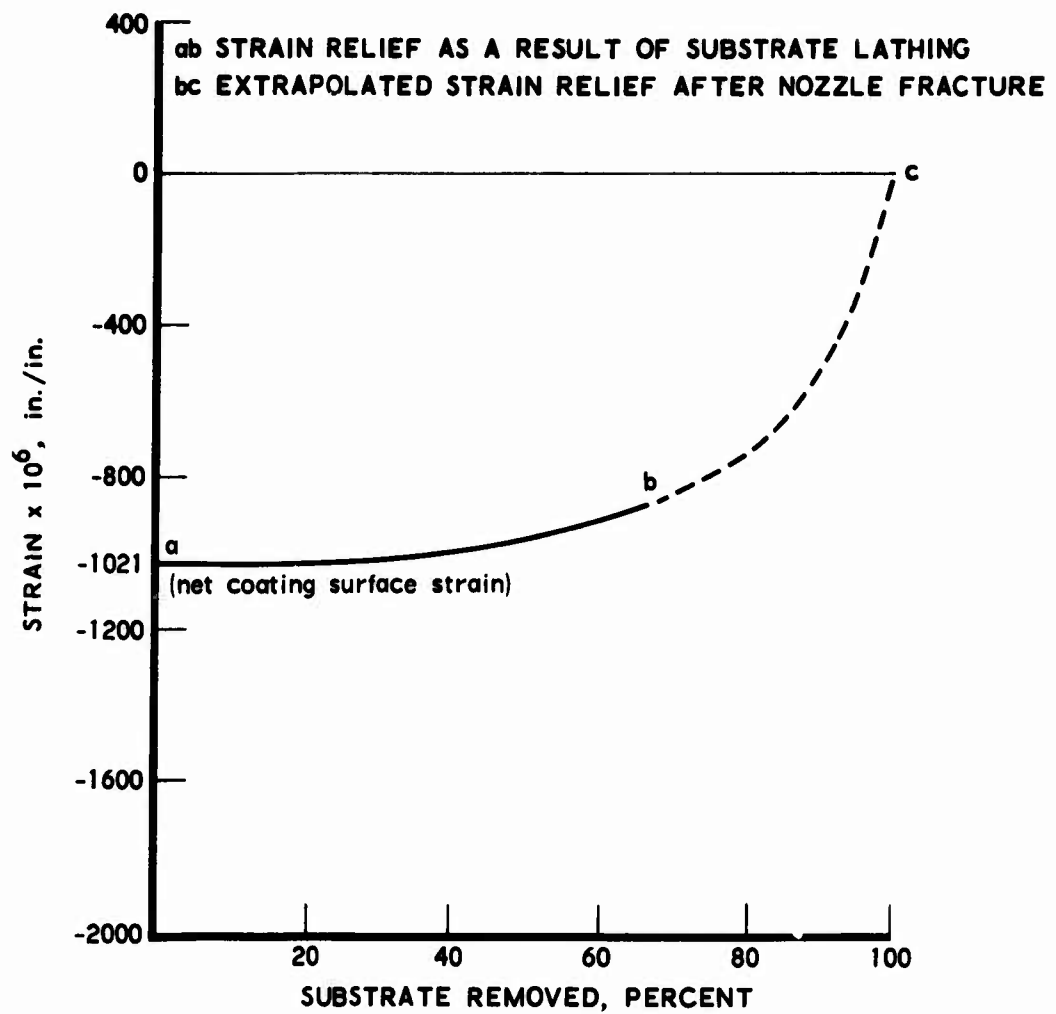
Fig. 18. Axial Strain Relief of PG Coating
Surface at Exit

Fig. 19. PG Coating Separated from ATJ Substrate
Showing Inside Diameter Tensile Failure
Incurred During Cool Down
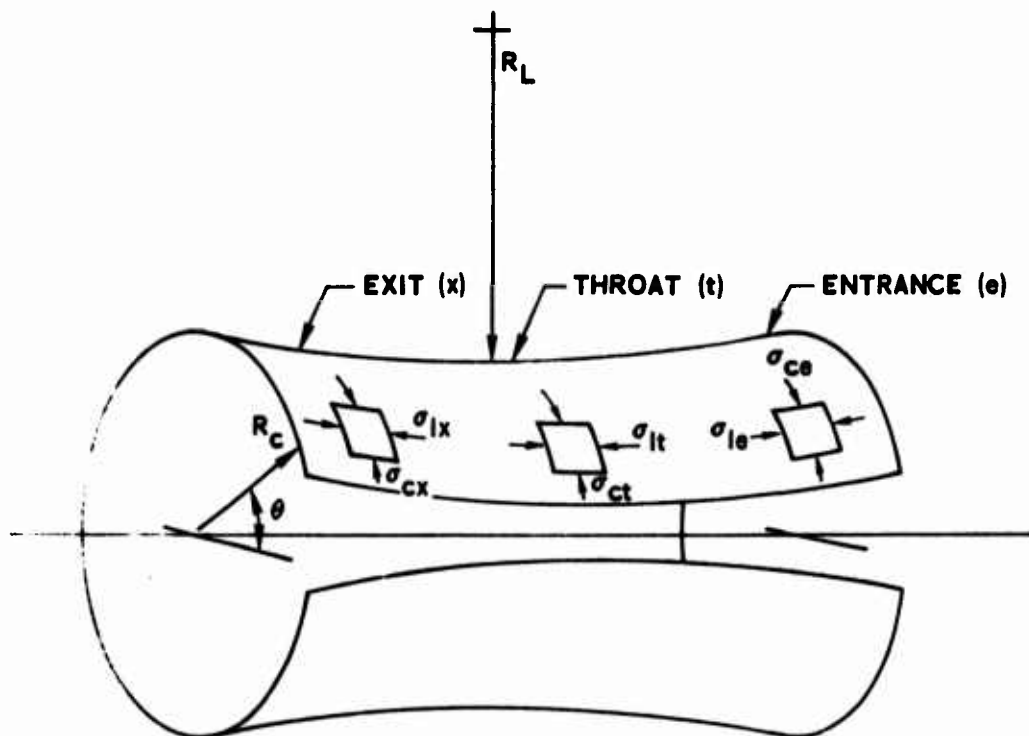
NOMENCLATURE

σ_{ce} CIRCUMFERENTIAL DIRECTION AT ENTRANCE
σ_{ct} CIRCUMFERENTIAL DIRECTION AT THROAT
σ_{cx} CIRCUMFERENTIAL DIRECTION AT EXIT

σ_{le} LONGITUDINAL DIRECTION AT ENTRANCE
σ_{lt} LONGITUDINAL DIRECTION AT THROAT
σ_{lx} LONGITUDINAL DIRECTION AT EXIT

(all stresses are represented in compression)

Fig. 20. Position and Direction of Stress
Components

Summaries of the calculated circumferential and longitudinal or axial stresses are presented in Tables 1 and 2. In each case, the first column represents data that were generated specifically on ARC PG. As such, it should result in values close to actual stresses. Conversely, the limited number of properties measurements makes the data somewhat suspect. The other three columns tabulate stresses calculated by use of the worst reported properties from a literature search (i.e., those properties that result in the highest stress), the best properties, and the properties most commonly reported for a continuously nucleated, although vacuum process, material. The wide disparity in the resultant stresses is indicative of the need for accurate material properties. As indicated in Tables 1 and 2, the ARC properties are close to the best reported case. This is consistent with both microstructural examination and thermal properties measurements that show the ARC material to be less anisotropic than most conventional

Table 1. Maximum Circumferential Residual Stresses at
Coating Surface for 13-in. Inside Diameter
Insert of Pyrolytic Graphite

Material Property Used		ARC (by SoRI)	Worst Reported	Best Reported	Most Common
a-b compressive, $E \times 10^{-6}$		2.78	5.6	2.18	3.5
a direction ν		-0.09	+0.25	-0.15	-0.1
Location	Net $\epsilon \times 10^6$	Stress (psi)			
	Circum-ferential	Axial			
Entrance	1373	883	-3625	-9530	-3530	-4545
Throat	1783	561	-4850	-11500	-4835	-6110
Exit	1879	1021	-5000	-12750	-4910	-6285

Table 2. Maximum Axial Residual Stresses at Coating
Surface for 13-in. Inside Diameter Insert
of Pyrolytic Graphite

Material Property Used			ARC (by SoRI)	Worst Reported	Best Reported	Most Common
a-b compressive, $E \times 10^{-6}$			2.78	5.6	2.78	3.5
a direction ν			-0.09	+0.25	-0.15	-0.1
Location	Net $\epsilon \times 10^6$		Stress (psi)			
	Circum-ferential	Axial				
Entrance	1373	883	-2125	-7325	-1925	-2635
Throat	1783	561	-1120	-6015	-855	-1354
Exit	1879	1021	-2385	-8910	-2105	-2945

PG's. In any event, even the use of the most commonly reported properties
to calculate the maximum stresses results in numbers within about 20 percent
of the ARC-generated data. Therefore, it is reasonable to conclude that the
maximum coating stresses are compressive at the exit plane and have a cir-
cumferential magnitude of about 5000 to 6000 psi and an axial magnitude of
2000 to 3000 psi.

2. SILICON CARBIDE AND PYROLYTIC GRAPHITE CODEPOSITED INSERT

The inside diameter surface of the codeposited SiC/PG rocket nozzle
insert was prepared by sanding it to a uniform smoothness with 180-grit
abrasive paper. Degreasing of the coating surface was accomplished by
means of a hydrocarbon solvent cleaner. The surface was then conditioned
with a mild phosphoric acid applied with cotton-tipped applicators. The
conditioning solution was rinsed from the graphite surface with acetone and

then with methanol. Removal of the solutions that may have been trapped in surface irregularities was achieved by drying the surface with hot air (125 to 150°F). The surface was then chemically prepared with a mildly alkaline solution, and again saturated, cotton-tipped applicators were used to apply the neutralizing solution. The neutralizing solution was rinsed, and hot-air dried in the steps previously described. This procedure for surface preparation was also used on the outside diameter of the surface of the codeposited coating ring after the removal of the substrate by lathing. The strain gages used to instrument the codeposited coating were 9 EA-06-125TM-120 gages and 15 EA-00-270TN-350 gages. The 270 TN series was used to instrument the inside diameter surface. The selection of these gages was based upon their ability to reach equilibrium temperature rapidly and their gage length (0.270 in.). The 125 TM series strain gages were applied to the outside diameter surface of the codeposited ring after the substrate was removed. M-Bond 200 (methyl-2-cyanoacrylate) was used as the strain gage adhesive. An air-drying acrylic coating was used to protect the gage from moisture and electrical leakage.

A 20-minute stability test was performed on each gage. Studies performed previously have shown that 20 minutes is a sufficient amount of time to indicate faulty adhesion to the graphite surface. If the gage showed instability, it was removed and replaced. The positioning of the gages on the surface of the codeposited rocket nozzle insert is shown in Fig. 21. A half-wheatstone bridge strain measuring system was used to minimize the temperature effects during each reading, i.e., one active gage was affixed to the nozzle insert being tested and one dummy gage to a codeposited rocket nozzle that was not tested.

A Vishay high-sensitivity, digital strain indicator with internal calibration, Model V/E-120, was used to measure the strain output. A 42-position switching box successfully eliminated contact resistances. The experimental setup prior to the first lathing cut is shown in Fig. 22. The strain gages were biaxial and aligned in axial (A) and circumferential (C) directions at the entrance, throat, and exit of the nozzle insert at 90-deg increments.
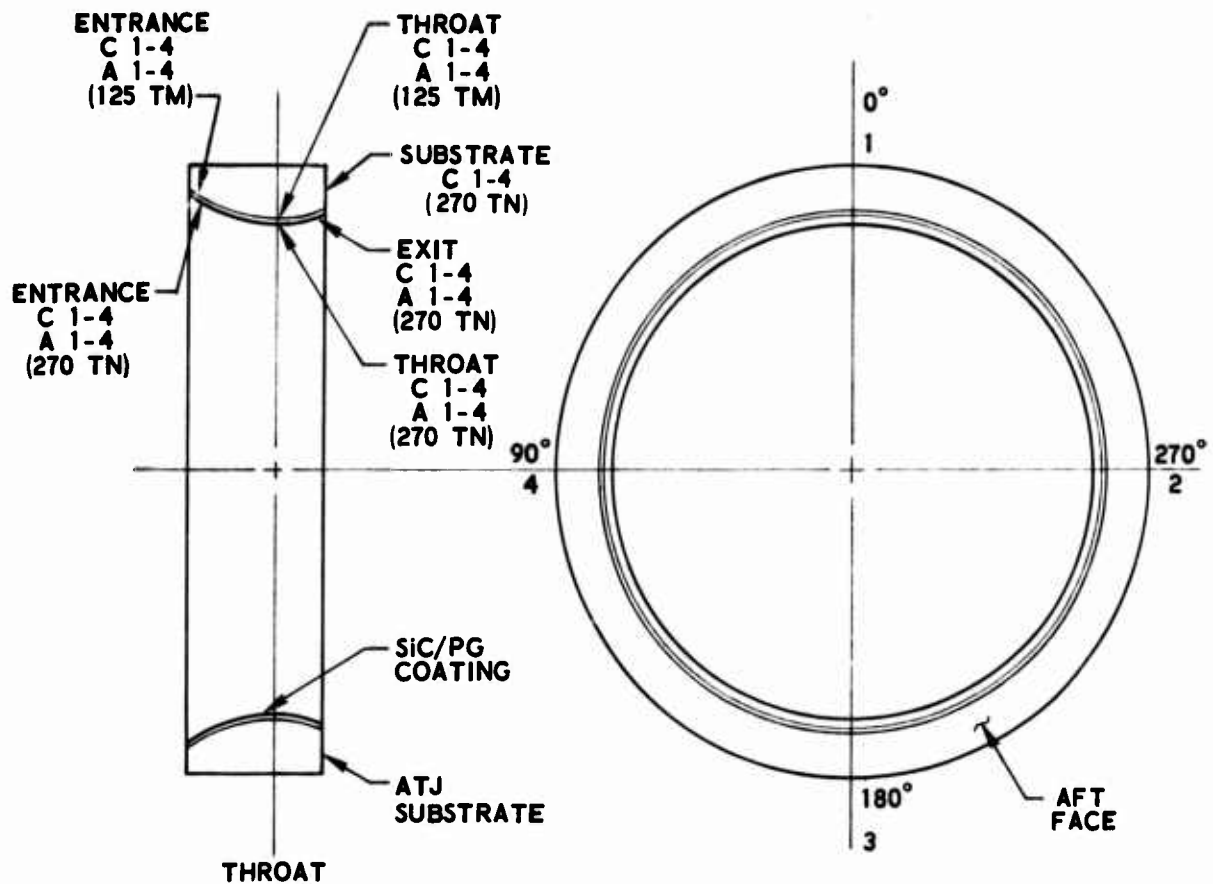
Fig. 21. Top and Section Views of SiC/PG Codeposit
Nozzle Indicating Strain Gage Positions
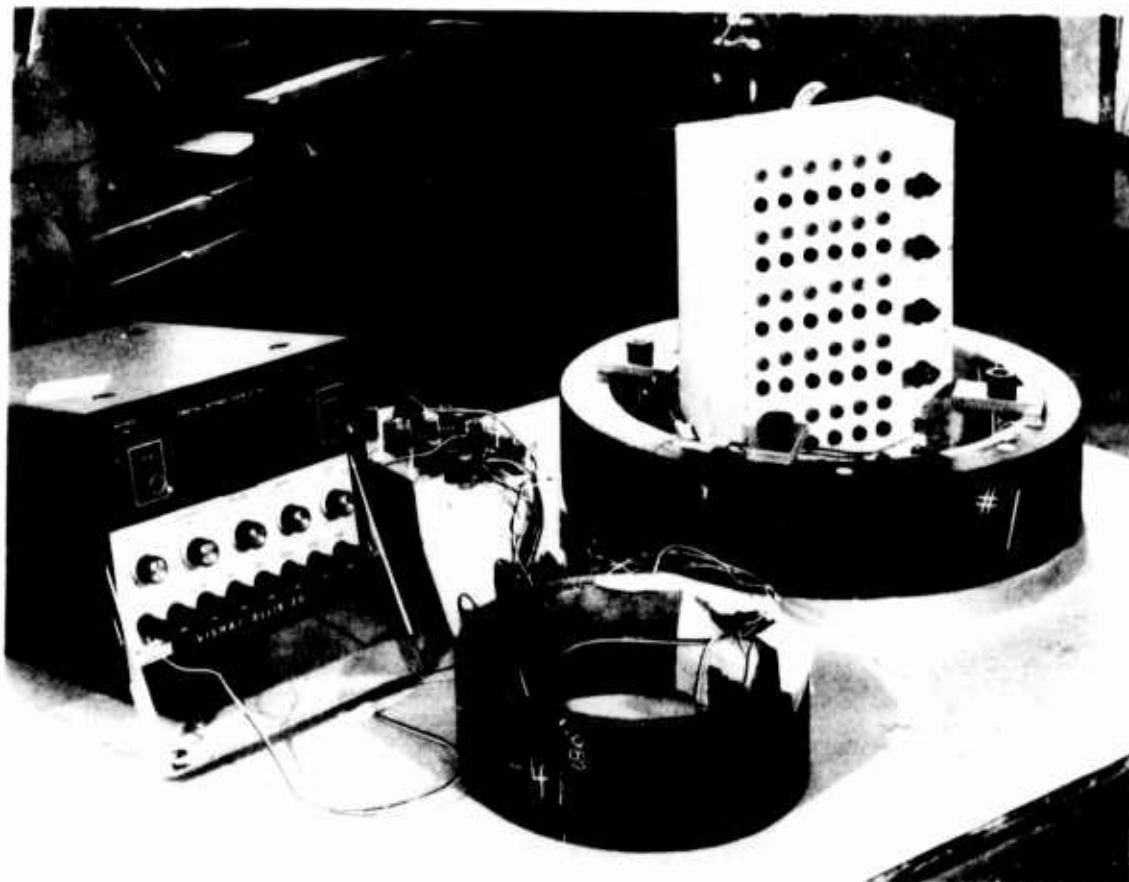
Fig. 22. Experimental Setup Showing the Codeposited SiC/PG
Nozzle Insert Being Readied for Lathing

Strain gages were also attached to the substrate material on the aft surface in 90-deg increments. The 125 TM strain gages were mounted on the outside diameter surface of the codeposited ring after the complete removal of the substrate.

The following procedure was performed to remove the ATJ substrate:

a.   Strain readings were taken from each gage.

b.   Nozzle insert was clamped into the fixture and placed into the lathe.

c.   0.050 in. was removed from the outside radius of the ATJ substrate.

d.   Nozzle insert and fixture were removed from the lathe and unclamped.

e.   Strain readings were taken.

This procedure was continued until further lathing would penetrate into the codeposited coating. At this point, the remaining substrate was removed by hand grinding. Strains of the now free-standing coating were measured, and the coating outside diameter was instrumented at stations complimentary to the inside diameter gages (see Fig. 21).

The codeposited shell was then split longitudinally, and the strain values read. This process was repeated, isolating the gage sets, until there was zero shift in the gage readings. Only three cuts were required.

The circumferential and axial strain data at the coating surface are shown in Figs. 23 through 28. As in the case of the PG insert, the data presented are an average of the values obtained at 90-deg locations (see Fig. 17). The stress reversal of the PG/AGSR insert was again evident, but opposite in direction. In the case of this SiC/PG codeposit, the coating surface stress of the composite reversed from tensile to compressive for the free-standing coating. The free-standing, codeposited coating before and after longitudinal sectioning is shown in Figs. 29 and 30, respectively. Also shown are the strain gages mounted on both surfaces of the coating. The stress profile opposite that of the PG insert is presented in Fig. 30 (see Fig. 19). The end points of the coating strain profile are listed in Table 3. No illustrative
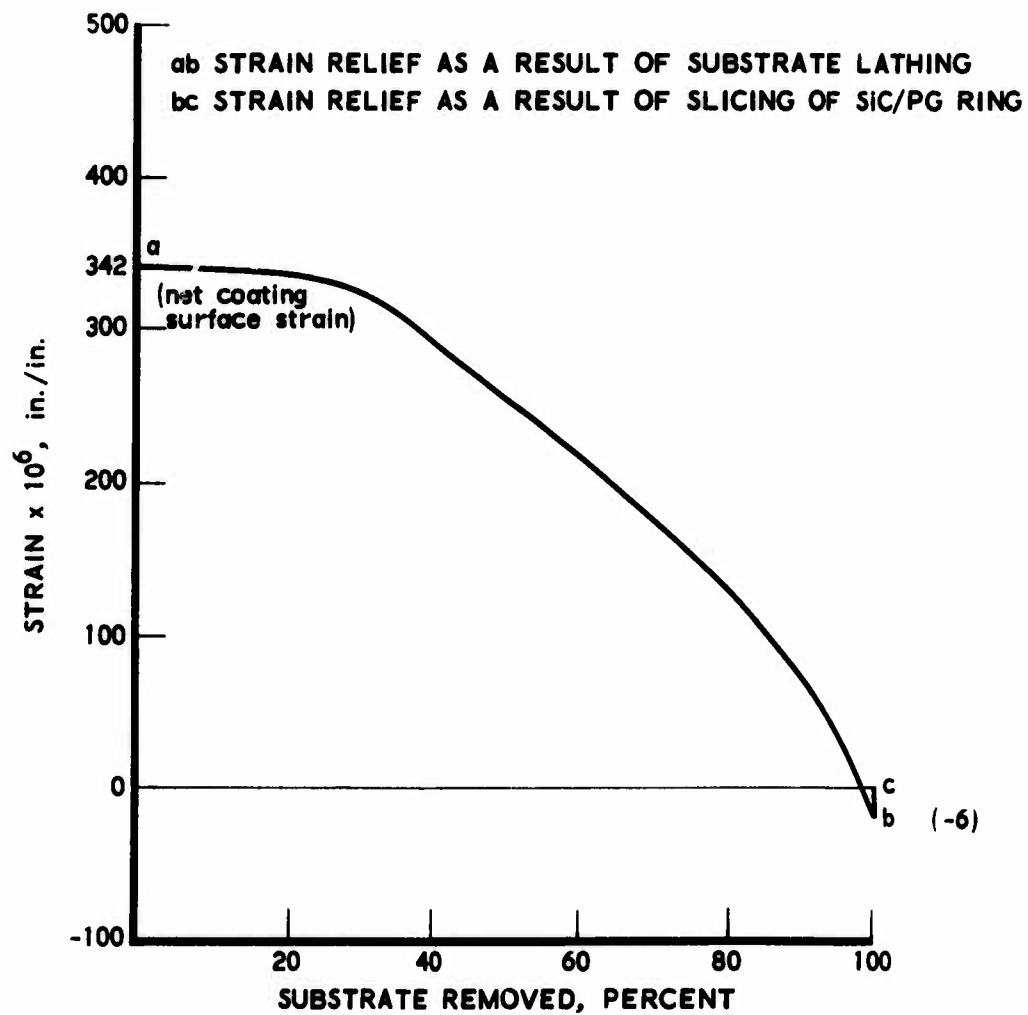
Fig. 23. Circumferential Strain Relief on Inside
Surface of SiC/PG Nozzle at Entrance
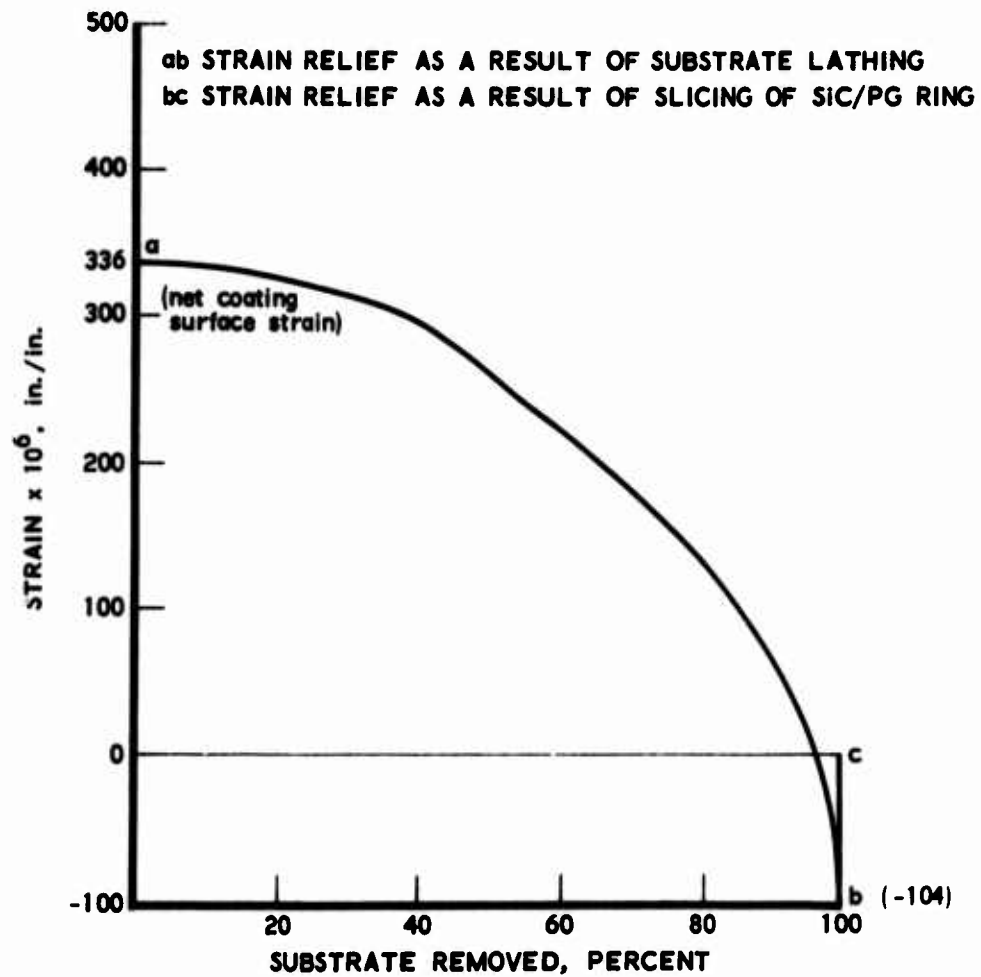
Fig. 24. Circumferential Strain Relief on Inside
Surface of SiC/PG Nozzle at Throat
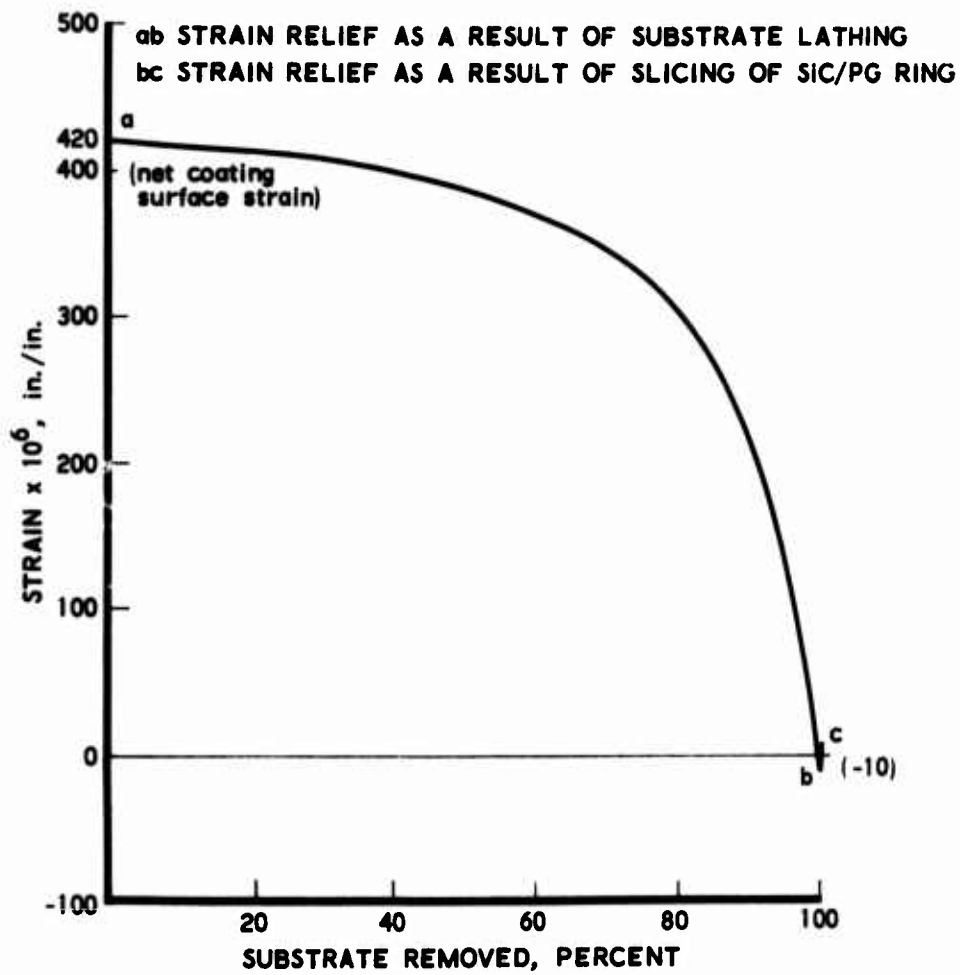
Fig. 25. Circumferential Strain Relief on Inside
Surface of SiC/PG Nozzle at Exit
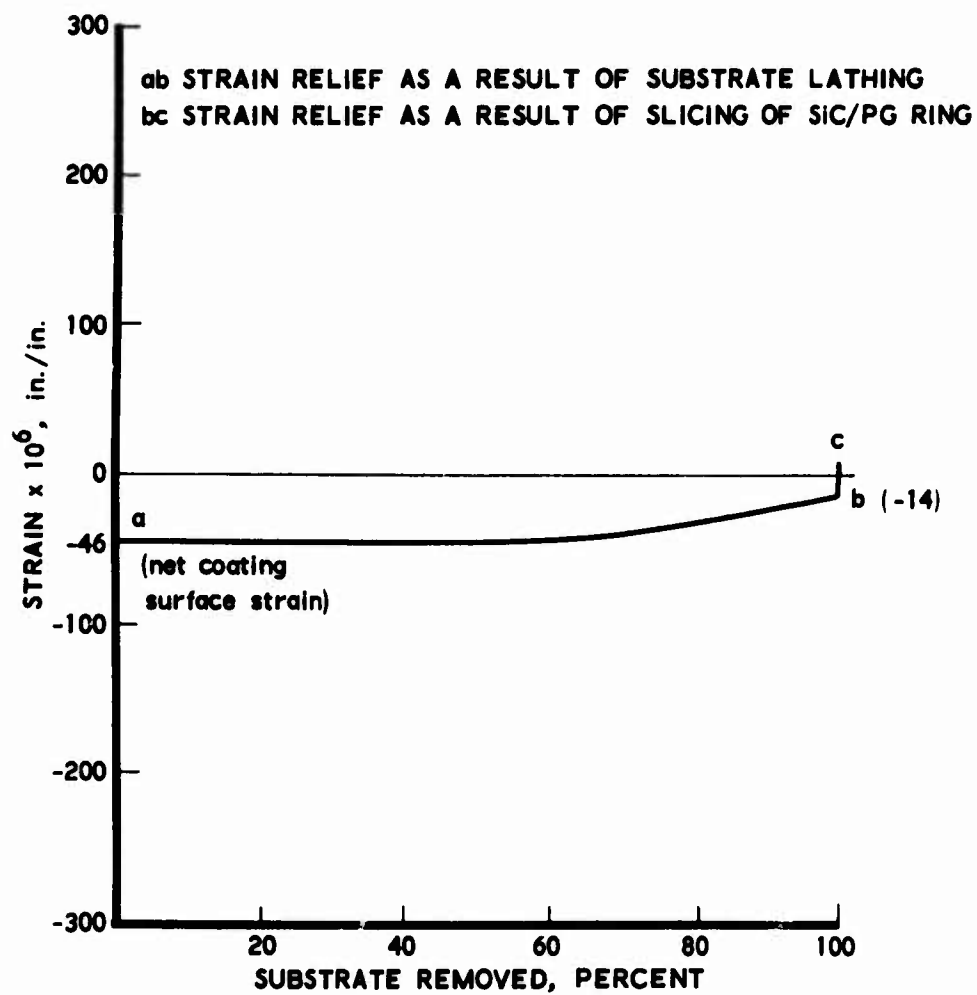
Fig. 26. Axial Strain Relief on Inside Surface of
SiC/PG Nozzle at Entrance
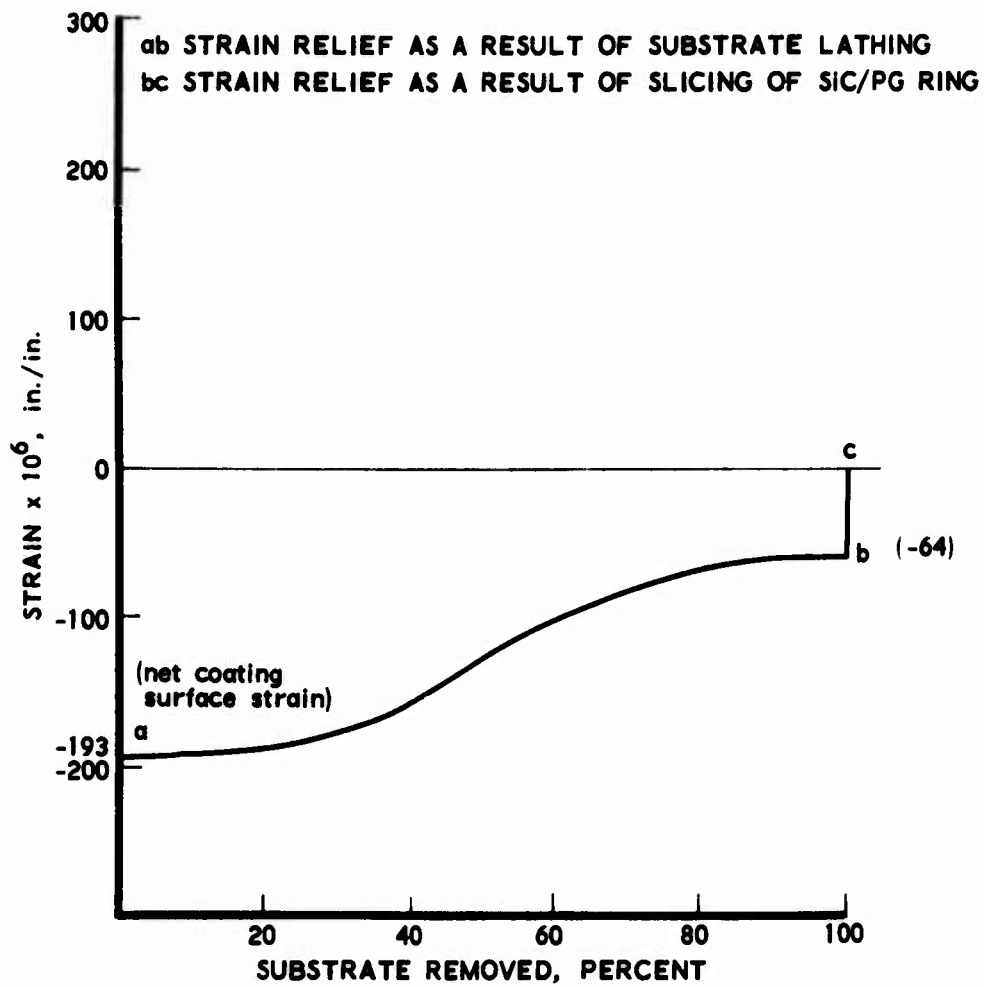
Fig. 27. Axial Strain Relief on Inside Surface of
SiC/PG Nozzle at Throat
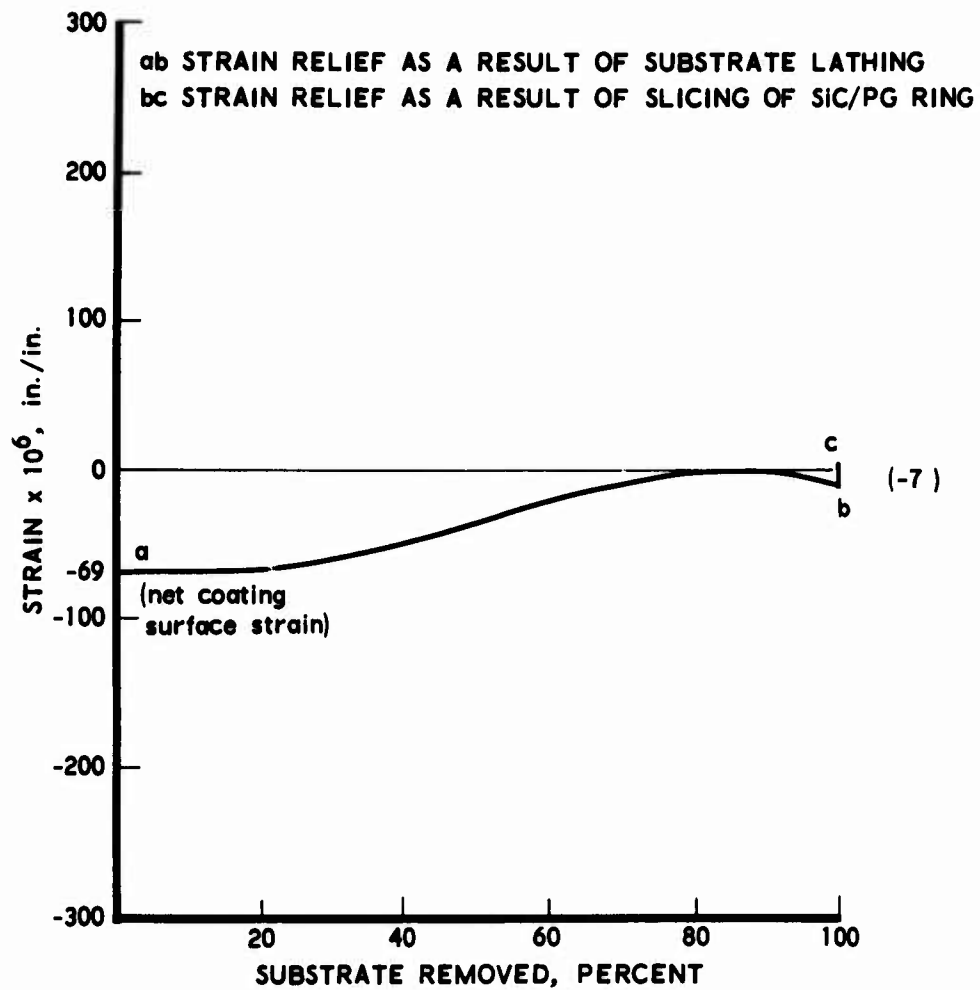
Fig. 28. Axial Strain Relief on Inside Surface of
SiC/PG Nozzle at Exit
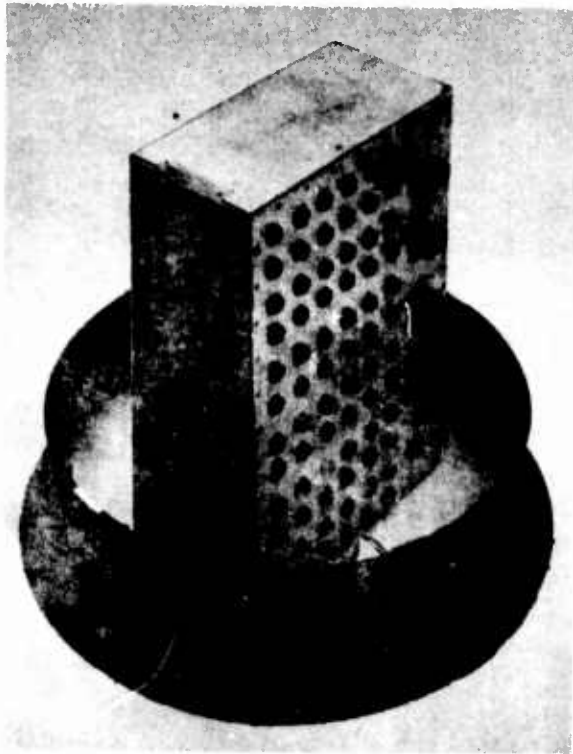
Fig. 29. Codeposited SiC/PG Coating with ATJ Substrate Completely Removed

Fig. 30. Codeposited SiC/PG Coating After Longitudinal Cut Showing Expansion in Ring Diameter
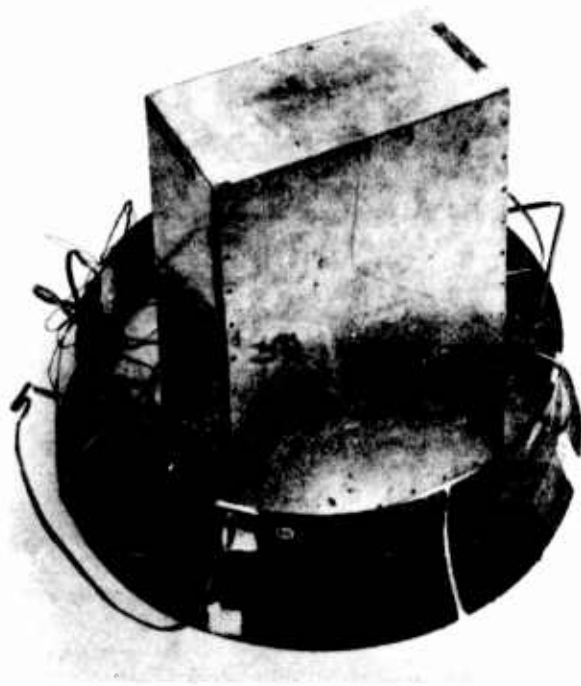
Table 3. Residual Strains on Inside and Outside of SiC/PG Codeposited Coating (Without Substrate)

Position	Residual Strain Inside Diameter Surface	Residual Strain Outside Diameter Surface
Circumferential		
Entrance	-10	+170
Throat	-104	+74
Exit	-20	+157
Axial		
Entrance	-13	-21
Throat	-64	+74
Exit	-14	-25

interpolation of this profile can be attempted with any degree of confidence because of the extreme complexity of the curve.

The same equation, derived as a variation of Hook's law, as was used to calculate the stresses of the PG insert was also used here. The assumptions employed in the deviation were also identical.

In order to determine the elastic modulus at each position (entrance, throat, and exit), a quantitative analysis was performed of the weight percent of SiC present in the codeposited SiC/PG shell. The elastic modulus of the codeposited shell is function of the SiC content. The weight percent of SiC and the associated elastic modulus for each position is listed in Table 4. The value of υ used to determine the residual stresses was independent of SiC content and constant at 0.14. Calculated residual stresses from the experimentally determined residual strains on the inside diameter surface of the codeposited SiC/PG coating are presented in Table 5.

Table 4. Weight Percent of Silicon Carbide
and Associated Elastic Modulus
for Location of Each Nozzle Insert

Position	SiC Weight Percent Average	$E \times 10^6$ psi Average[a]
Entrance	24.28	5.2
Throat	20.76	4.7
Exit	18.48	4.0

[a]a-b tensile and compressive

Table 5. Maximum Residual Stresses at Coating Surface
for 12-in. Inside Diameter Insert of SiC/PG

Direction	Location	Substrate-Induced Stress (psi)	Coating Isolated Stress (psi)	Net Stress (psi)
Circumferential	Entrance	1900	-120	1780
	Throat	2025	-542	1483
	Exit	1730	-50	1680
Axial	Entrance	100	-90	10
	Throat	-321	-379	-700
	Exit	19	-60	-41

From these data, we can conclude that the maximum residual stress in this SiC/PG codeposited coating at the surface is under 2000 psi and tensile.

B.   THERMAL EXPANSION

During this reporting period, characteristic thermal expansion curves for the a-b plane and c axis were developed from room temperature to 5000°F for several key graphite coatings. One of these materials, a UK PG coating, was examined to evaluate the effect of cyclic heating on the general thermal expansion curve and the resultant change in the coefficient of thermal expansion (CTE). The thermal expansion characteristics were compared with the degree of graphitization within the material. The c axis thermal expansion was measured for an 18 percent SiC/PG codeposited sample and the results were compared with the data generated by the Southern Research Institute (SoRI). A literature search was conducted of existing high-temperature thermal expansion data for other PG coatings, and these data were compared with the measured data. In addition, a survey was made of thermal expansion measurements that have been conducted on various carbon-carbon systems as a part of current reentry programs. These data are compared with the measured coatings data.

The objectives of this portion of the program were: (1) to establish thermal expansion profiles for some new coating materials, (2) to compare the ARC PG and the UK PG with others of the class (Super Temp, HTM, Pfizer, etc.), and (3) to compare the coatings expansion with some potential substrate candidate for compatibility.

A Leitz model VBD quartz dilatometer was employed for expansion determinations from room temperature to 1100°C (the upper limit of the equipment). Above 1100°F, a graphite tube furnace was utilized with optical techniques for determining expansion. Dwell times were fixed at 15 min and held constant for each material. The optical device was a Gaertner tele-microscope with 50×10^6 divisions/in. In all cases, runs were made under

an argon atmosphere and at ambient pressure. The dilatometer data were generated in a continuous automated process in which $\Delta l/l_o$ x-y plots were inscribed on light-sensitive film.

Thermal expansion vs temperature for a sample of UK PG in the a-b plane and c axis are shown in Figs. 31 and 32, respectively. The initial contraction to approximately 800°F and the extremely low a-b plane CTE $(0.78 \times 10^{-6}$ in./in./°F between 0 to 2000°F and between 1800 and 3500°F) are characteristic of the high degree of anisotropy that is associated with this type of substrate nucleated material deposited at 2000°C and under vacuum. The c axis CTE is also representative of a highly anisotropic structure. The CTE of 0 to 2000°F is 14.1×10^{-6} in./in./°F and the resultant $\alpha c/\alpha ab$ is 18:1, which is well over the 10:1 "average" reported in the literature. In order to show more dramatically the degree of anisotropy that this material possesses, the UK thermal expansion curve for the a-b plane is compared in Fig. 33 with a compilation of all reported a-b expansion data that were uncovered in a brief literature search of other pyrolytic graphites, together with an experimentally determined $\Delta l/l_o$ - temperature curve of an ARC PG sample (009-48). Comparable data for the c axis expansion are shown in Fig. 34.

A piece of the UK PG was graphitized to Stage I by heat treating the material at 2750°C for 1 hr. (The temperature-time relationship was determined from experimentation that is discussed in Sec. IIC of this report.) Stage I was successfully achieved, as indicated by measurement of unit cell height C_o spacing, which shifted from 6.8176 to 6.7416 Å as a result of the heat treatment. A thermal expansion vs temperature curve was generated for this heat-treated UK PG on the dilatometer in the a-b plane. The purpose of this experiment was to examine the effects of thermal loading on anisotropy; the resulting $\Delta l/l_o$ vs temperature curve and the as-deposited curve are plotted in Fig. 35. The reduction in a-b expansion is marked. The CTE of the Stage I graphitized material for the temperature range of room temperature to 2000°F is 1/10 that of the as-deposited material.

This measured reduction in a-b plane CTE is in agreement with earlier experimental studies (Refs. 3 and 4). For long-duration, high-temperature, rocket motor firing, this response could imply a problem with "in-depth" shear failure that manifests itself as massive internal delamination.

The thermal expansion of a CH_4 vacuum deposition by Pfizer was measured. This commercial material was selected as being representative of the PG in current usage for Trident I. The thermal expansion in the a-b direction as a function of temperature is shown in Fig. 36. In general, the material behaves similarly to the UK PG in terms of thermal expansion. It had a CTE of 0.8×10^{-6} in./in./°F from room temperature to 2000°F and 0.9×10^{-6} in./in./°F from 1500 to 3500°F, which is near the lower end of the a-b plane CTE curve (see Fig. 33).

An experimental check of the procedure was made by determining the thermal expansion of an 18 percent SiC/PG codeposited sample and comparing it with data generated by SoRI for a comparable percent SiC/PG sample. The good correlation with SoRI-generated data is shown in Fig. 37.

In addition to the foregoing experimental procedures, a literature search was made of all thermal expansion vs temperature data for carbon-carbon heat shield and nose-tip candidate materials. This effort was felt to be pertinent in light of the desire to examine carbon-carbons as a potentially higher tensile strength, more compliant substrate material for PG coatings. Some of the more interesting curves plus a range of PG thermal expansion curves are shown in Fig. 38.

C. MICROSTRUCTURE

The measurement of C_o is a convenient way to examine the response of an ordered crystallite structure, such as PG, to thermal exposure above temperatures that induce reordering of the lattice. This structure ordering, or degree of graphitization, is important in that some key thermal and mechanical properties of the PG are extremely sensitive to this ordering, and they, in turn, affect the overall stress state of a given nozzle throat insert. Thus, for each level of C_o, there is a family of associated material properties,
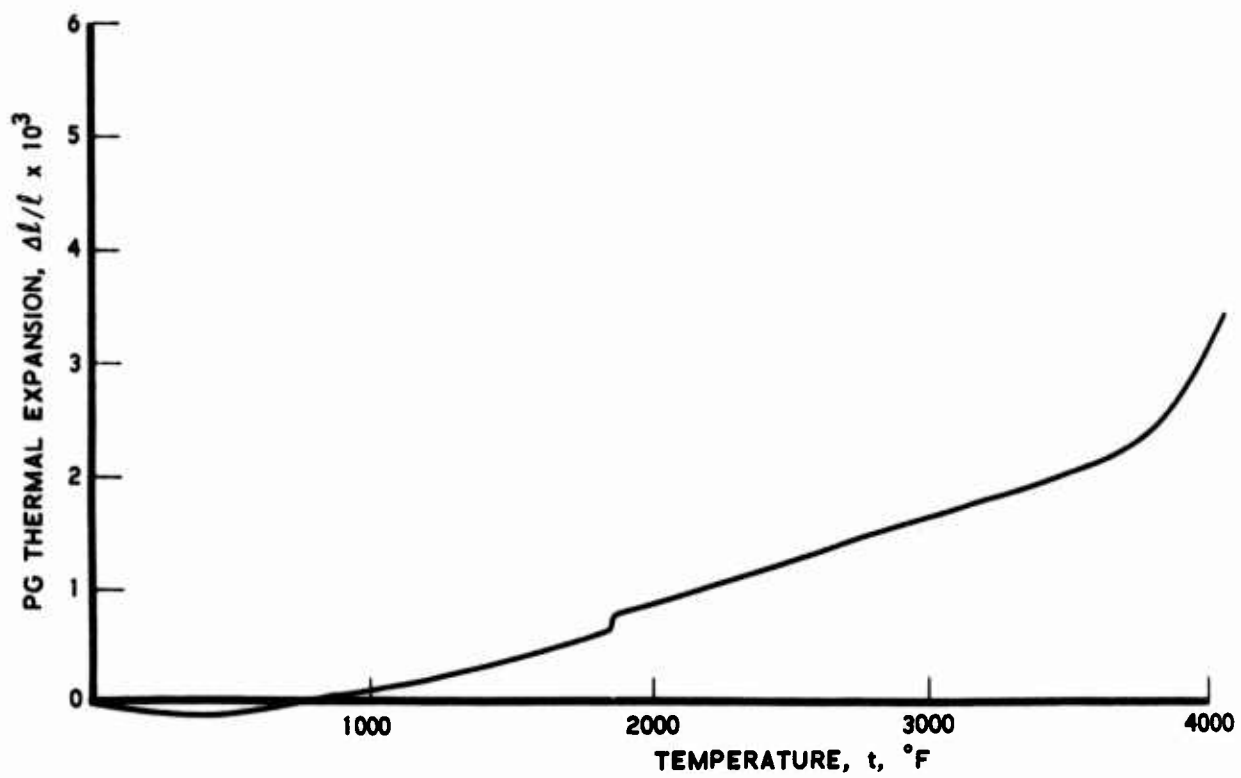
Fig. 31. Thermal Expansion of a-b Plane vs
Temperature of UK PG
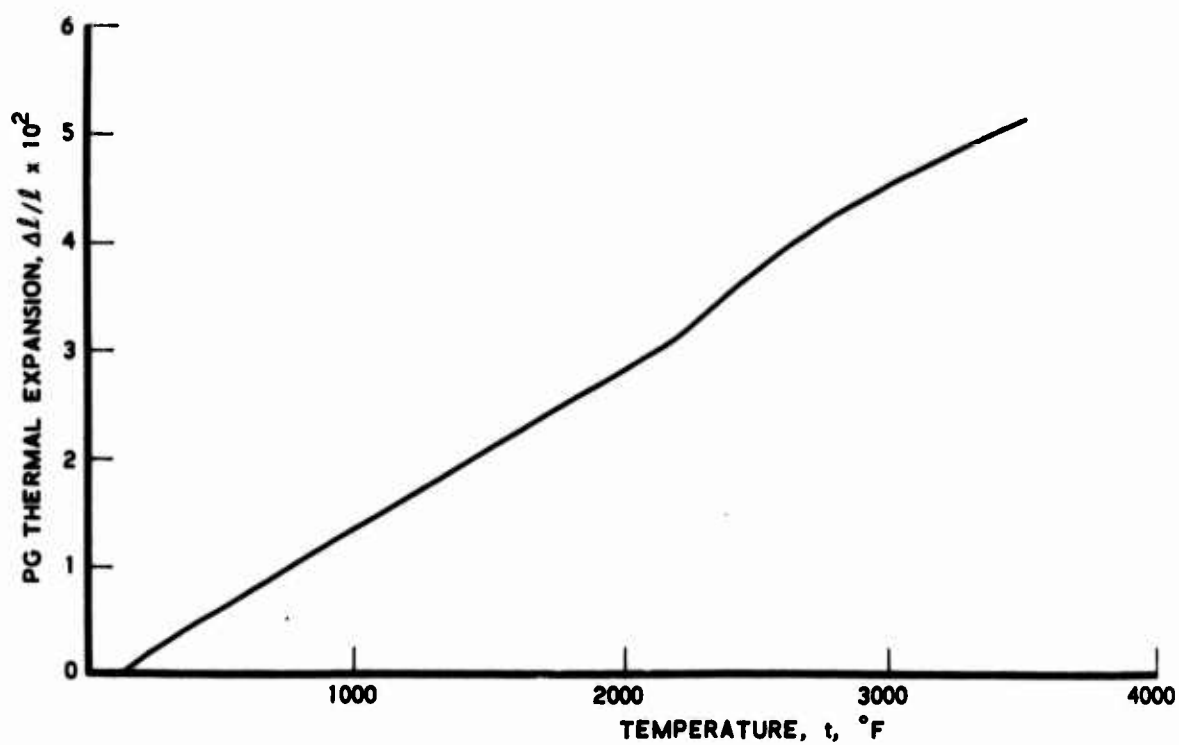
Fig. 32. C Axis Thermal Expansion vs Temperature
of UK PG
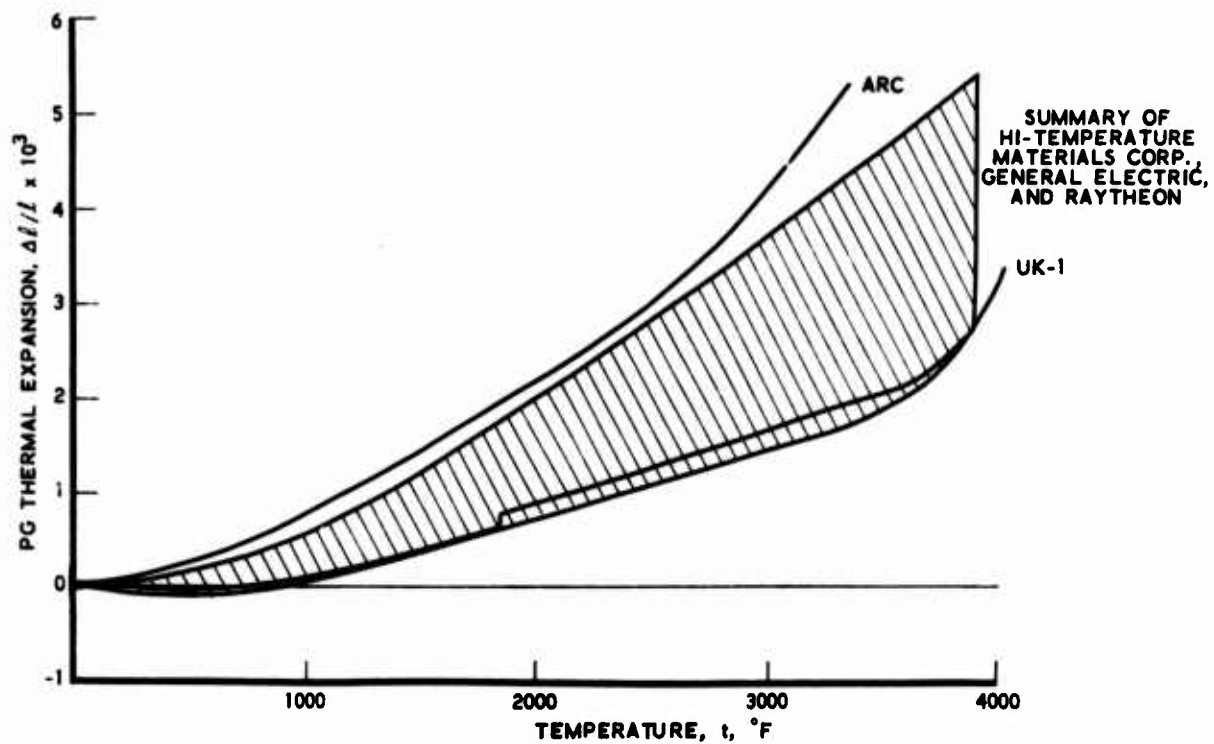
Fig. 33. Thermal Expansion of a-b Plane vs Temperature
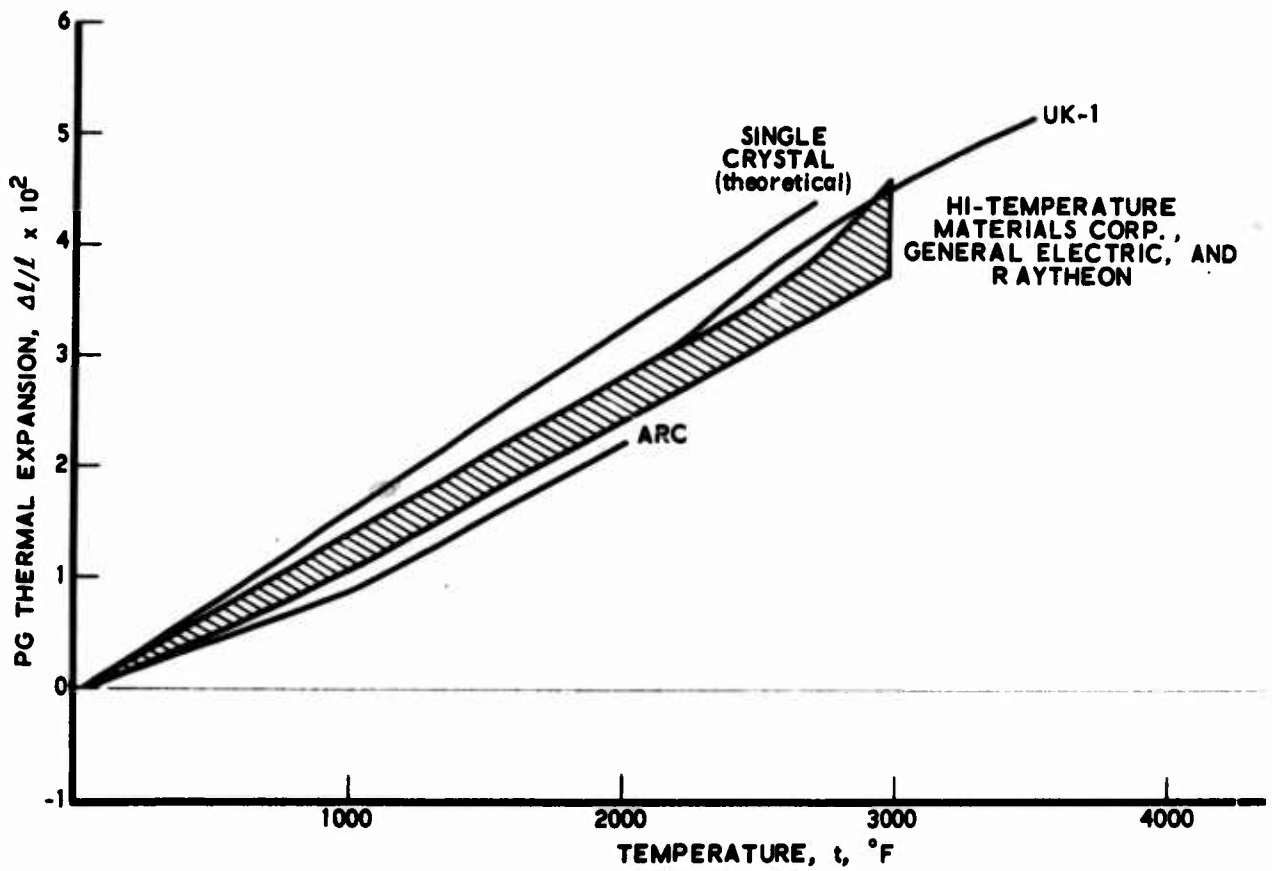
Fig. 34. C Axis Thermal Expansion vs Temperature

Fig. 35. Thermal Expansion of a-b Plane vs Temperature
for As-Deposited and Stage I Graphitized UK PG

Fig. 36. Thermal Expansion of a-b Plane vs Temperature
of Pfizer PG

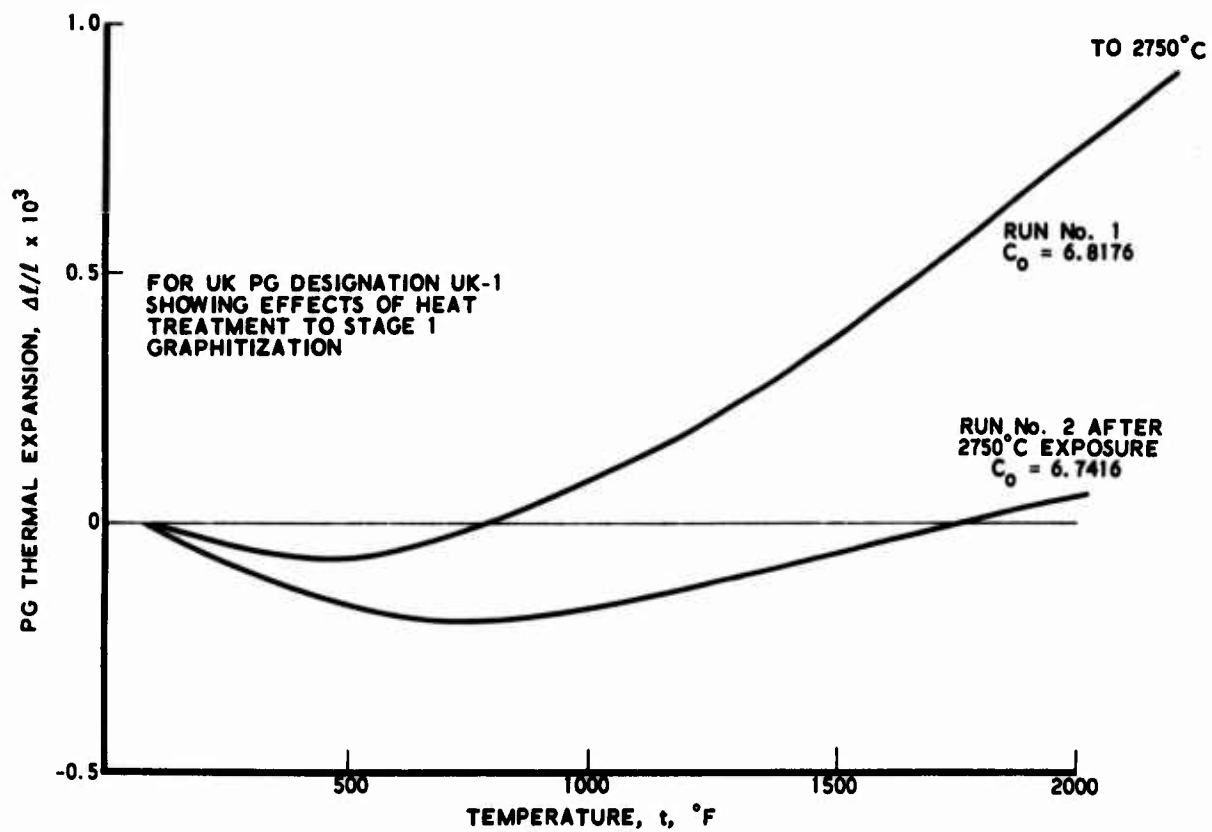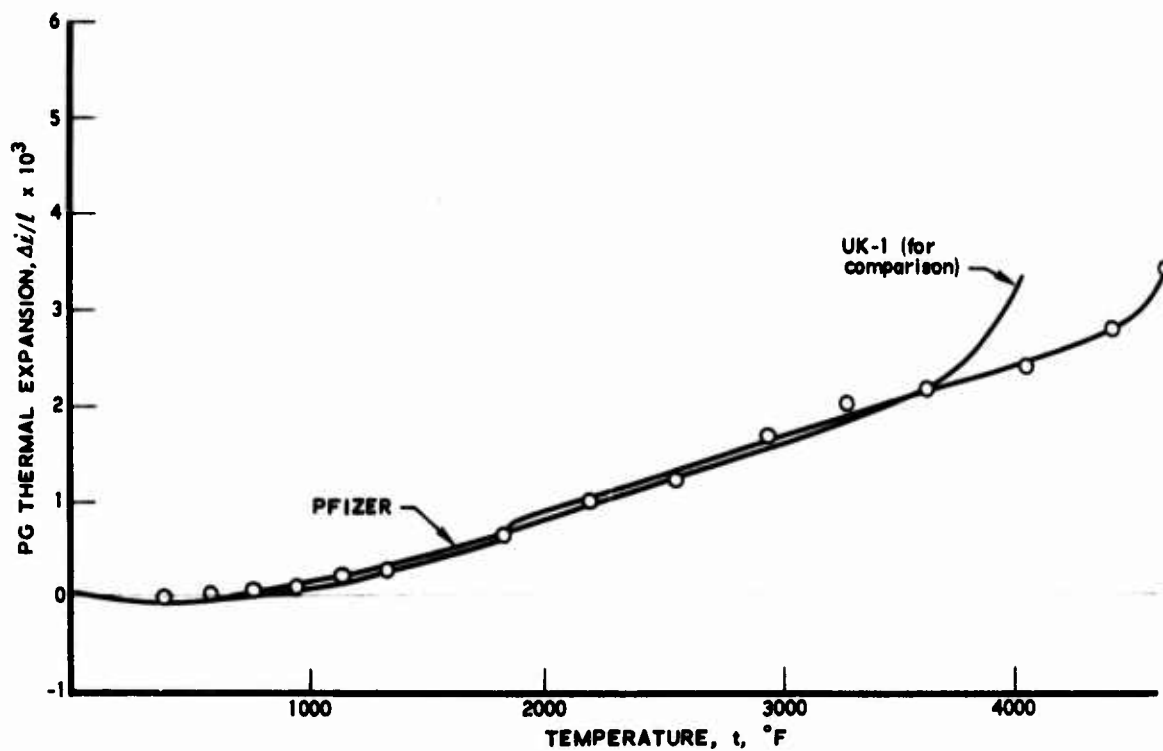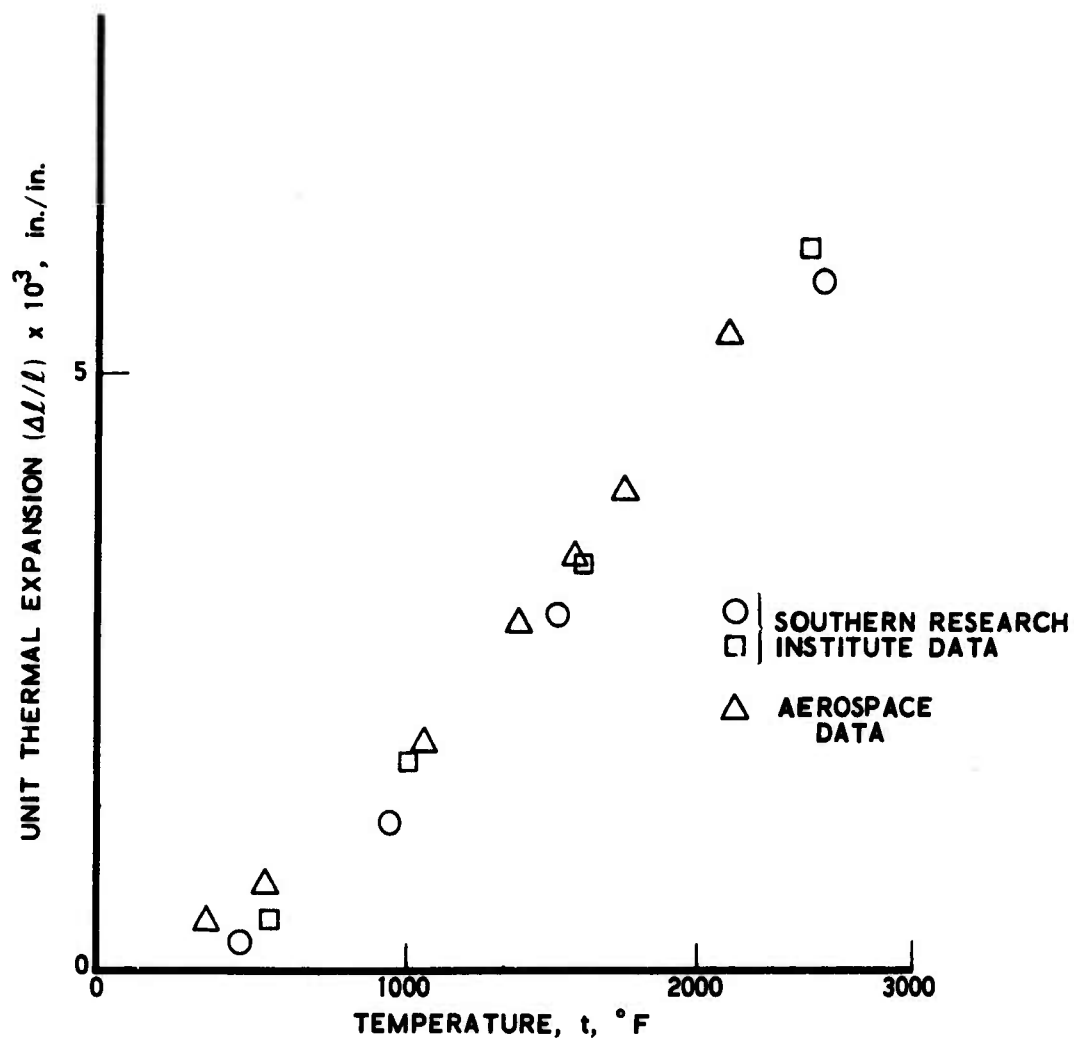Fig. 37. Thermal Expansion of Codeposited Pyrolytic
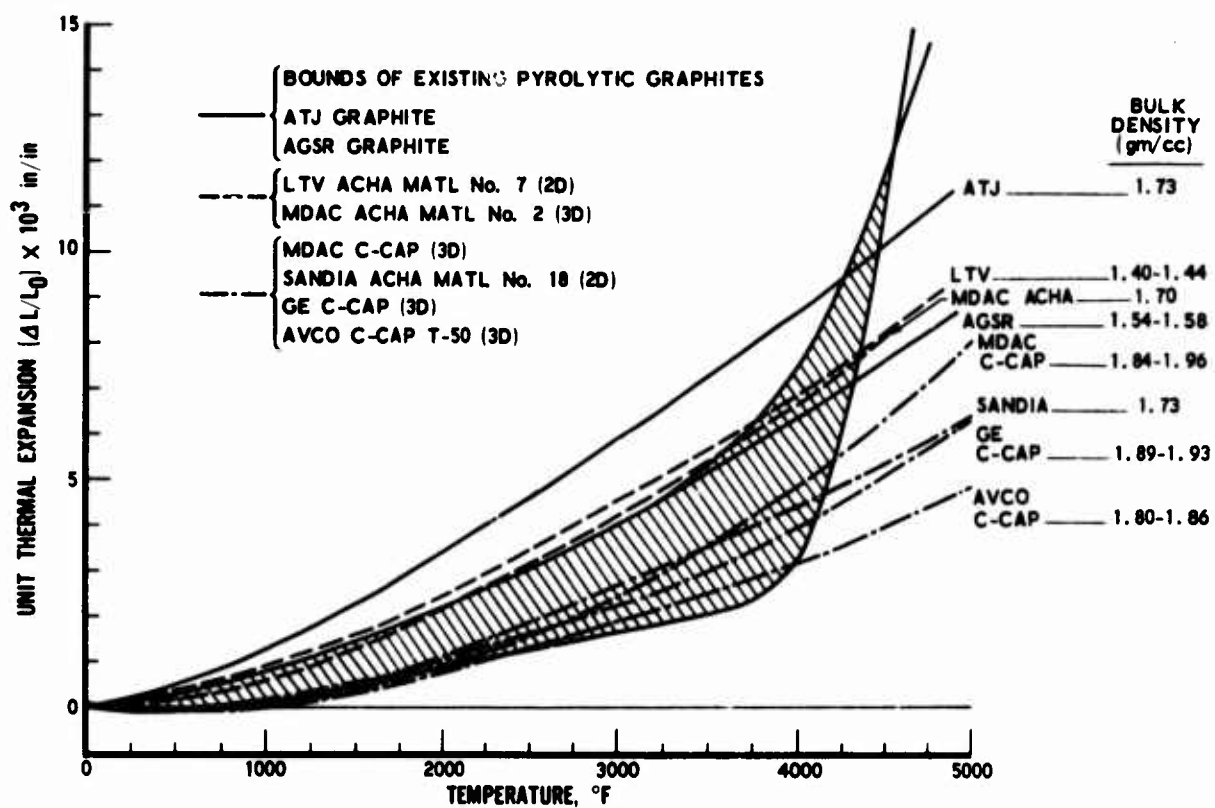Graphite with 18-Percent SiC in the
C Direction

Fig. 38. Circumferential Thermal Expansion vs Temperature
Comparison of Pyrolytic Graphites with Reentry
Carbon-Carbon and Polycrystalline Graphites

and, for general purposes, it is an easier task to monitor C_o than to define all the key properties.

Some of the C_o studies were actually conducted prior to this reporting period under an Aerospace-funded project, but are included here in order to maintain continuity of the overall study. A summary of the C_o measurements is given in Table 6. This summary is shown in visual form in Fig. 39, which illustrates the time dependence of the cell height-temperature relationship. From the limited data available, it is difficult to draw a meaningful conclusion relative to the effects of a rocket motor exposure on the PG microstructure. Indications are that the reduction of unit cell height is inhibited by the single-face heating of a motor firing. Conversely, some shifting of the cell structure is apparent, especially for the longer run times where the thermal gradient across the coating is reduced. This trend is illustrated in Fig. 39, which shows the shift of the most graphitized structure from the substrate to flame front during firing. In all cases of as-deposited material, the substrate or first deposit surface exhibited the greatest degree of graphitization. This was to be expected given the time dependency of the lattice ordering effect, and verifies earlier experiments by Stover (Ref. 4), Smith and Leed (Ref. 5), and others. Conversely, it was anomalous that there was such a disparity of results from the two relatively high-temperature nozzle tests. The UK PG showed little or no effects of graphitization, while a Super Temp PG coating was graphitized through Stage I reordering. This result occurred in spite of the fact that the Super Temp coating was exposed to a test of lower temperature and shorter duration (Fig. 39). The lack of data on long-duration (>60 sec), high-temperature (>6000°F), rocket motor firings, or a realistic means of simulating this type of heating, is the current deterent from additional efforts in this area.

Samples of several coatings of codeposited SiC/PG that had been subjected to the TRW thermal stress test were measured for C_o shift in an attempt to evaluate the material microstructural response to short-duration, high-flux heating. Unfortunately, the times (and the maximum surface temperatures) that were achieved were far short of those in which predictable

Table 6. Summary of Pyrolytic Graphite Unit Cell Height

Manufacturer	ARC				RPE		P_f				ST	
Source Gas/Coating	CH$_4$/PG		CH$_3$SiCl$_3$/SiC-PG		C$_2$H$_2$/PG		C$_2$H$_2$/PG		CH$_4$/PG		CH$_4$/PG	
Deposition Pressure	1 ATM		1 ATM		VAC		VAC		VAC		VAC	
Material Configuration[a]	C	P	C	P	C	P	C	P	C	P	C	P
Side[b]												
As-Deposited C_o												
Rocket Motor 5600°F/30 sec — 1	6.842	6.854	6.810	X	6.866	X	X	6.848	X	6.852	6.844	6.842
5600°F/30 sec — 2	6.832	6.846	X	X	6.856	X	X	6.842	X	6.828	X	6.834
Heat-Treated C_o												
5600°F/80 sec — 1	6.818	X	X	X	X	X	X	X	X	X	X	X
5600°F/80 sec — 2	6.822	X	X	X	X	X	X	X	X	X	X	X
6175°F/16 sec — 1	X	X	X	X	X	X	X	X	X	X	6.728	X
6175°F/16 sec — 2	X	X	X	X	X	X	X	X	X	X	X	X
6500°F/28 sec — 1	6.860	X	X	X	X	X	X	X	X	X	X	X
6500°F/28 sec — 2	X	X	X	X	X	X	X	X	X	X	X	X
80-Sec Laboratory 2800°C — 1	6.752	X	X	X	6.772	X	X	6.822	X	6.832	X	X
2800°C — 2	6.734	X	X	X	6.764	X	X	6.812	X	6.822	X	X
3000°C — 1	X	X	X	6.726[c]	6.752	X	X	6.722	X	6.720	X	X
3000°C — 2	6.712	X	X	6.726[c]	6.744	X	X	6.712	X	6.716	X	X
1-Hr Laboratory 2750°C — 1	X	X	X	X	6.742	X	X	X	X	X	X	X
2750°C — 2	X	X	X	X	6.741	X	X	X	X	X	X	X

[a] C-coating, P-plate

[b] 1- Last deposit/flamefront
2- First deposit/madrel-substrate

[c] 3038°C (5500°F)/20 sec at SoRI

C_o shifts would occur. No C_o shifts were measured for the two TRW samples that were examined, Nos. 4 and 8. As indicated in Figs. 40 and 41, neither specimen saw much more than a maximum of 4000°F, and that was only after a run of 10-sec duration. These values are far short of those necessary to achieve significant graphitization of the PG structure, with or without the presence of SiC.

In addition to the C_o measurements, a preliminary examination was made of a PG mode or gradient coating fabricated by the Materials Technology Corporation (MTC) of Dallas, Texas. The effects of processing changes on the PG structure are shown in Figs. 42 through 44. A photomicrograph of the polished entrance, which was taken with polarized light and magnified 100 times, is shown in Fig. 42. It illustrates the transition from the initial substrate nucleated structure to a highly regenerative material at the insert coating surface. The initial structure is characterized by intraconical delaminations that, in the larger growth cones, extend into the renucleated material. The deposition run had been stepped four times over a 2-hr period, with the temperature and flows of methane increased non-linearly. Deposition temperature range was 3800 to 4200°F. The ultimate coating was 54 mils thick and had a density of 2.22 g/cm^3. The substrate utilized was ATJ graphite. A view of the exit magnified 100 times is presented in Fig. 43, which shows a rather interesting anomalous condition that appears to be an a-b plane tensile failure. This area is magnified 1000 times in Fig. 44, which illustrates the high degree of misordering around the failure zone and locally reduced density. It is interesting to note that, in the exit plane, the PG exhibits a continuously renucleated structure from the substrate surface as opposed to the gradient structure at the entrance. Although this material sample was not without defects, it is perhaps significant in that the fabricator (MTC) has demonstrated that the process can be "tailored" to fit what may be analytically determined as an optimum stress state for the insert structure.
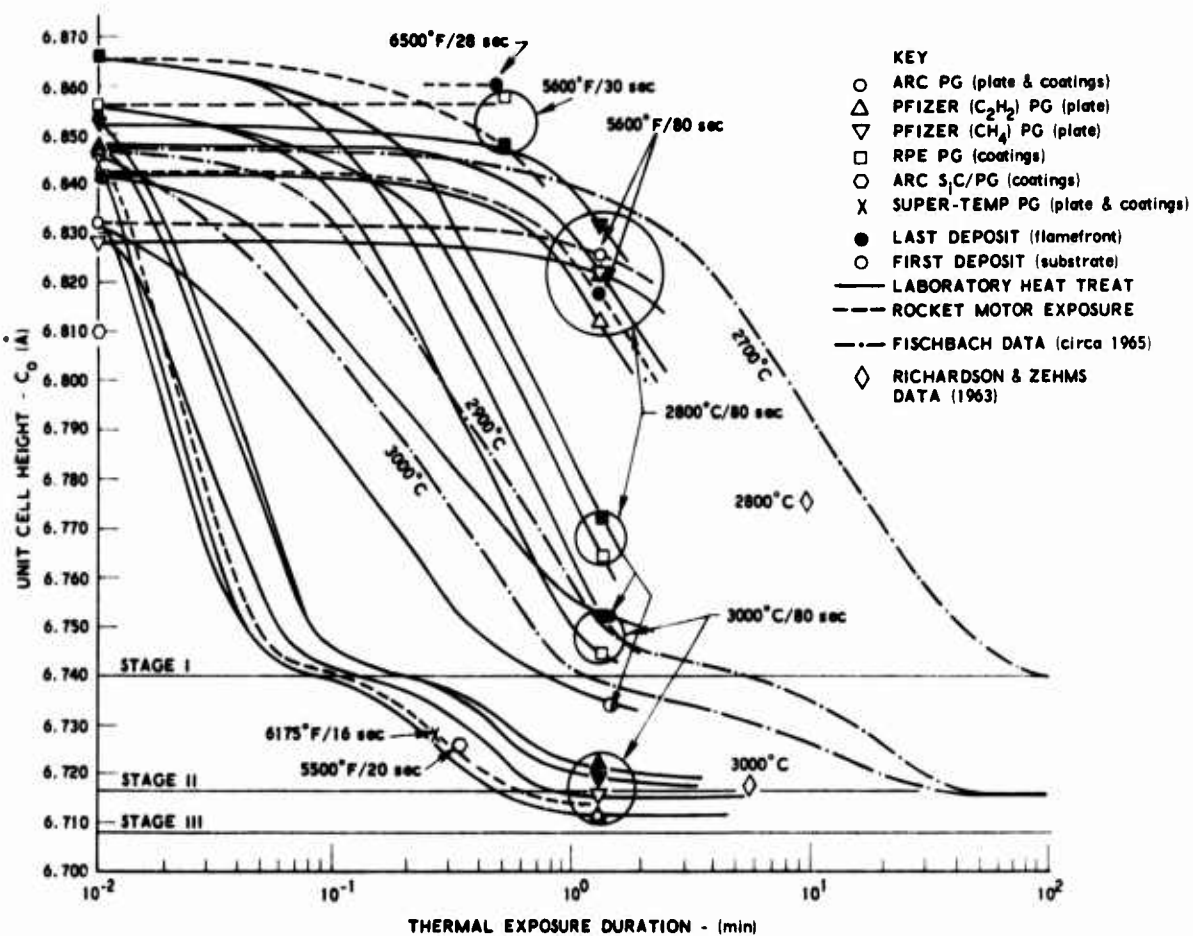
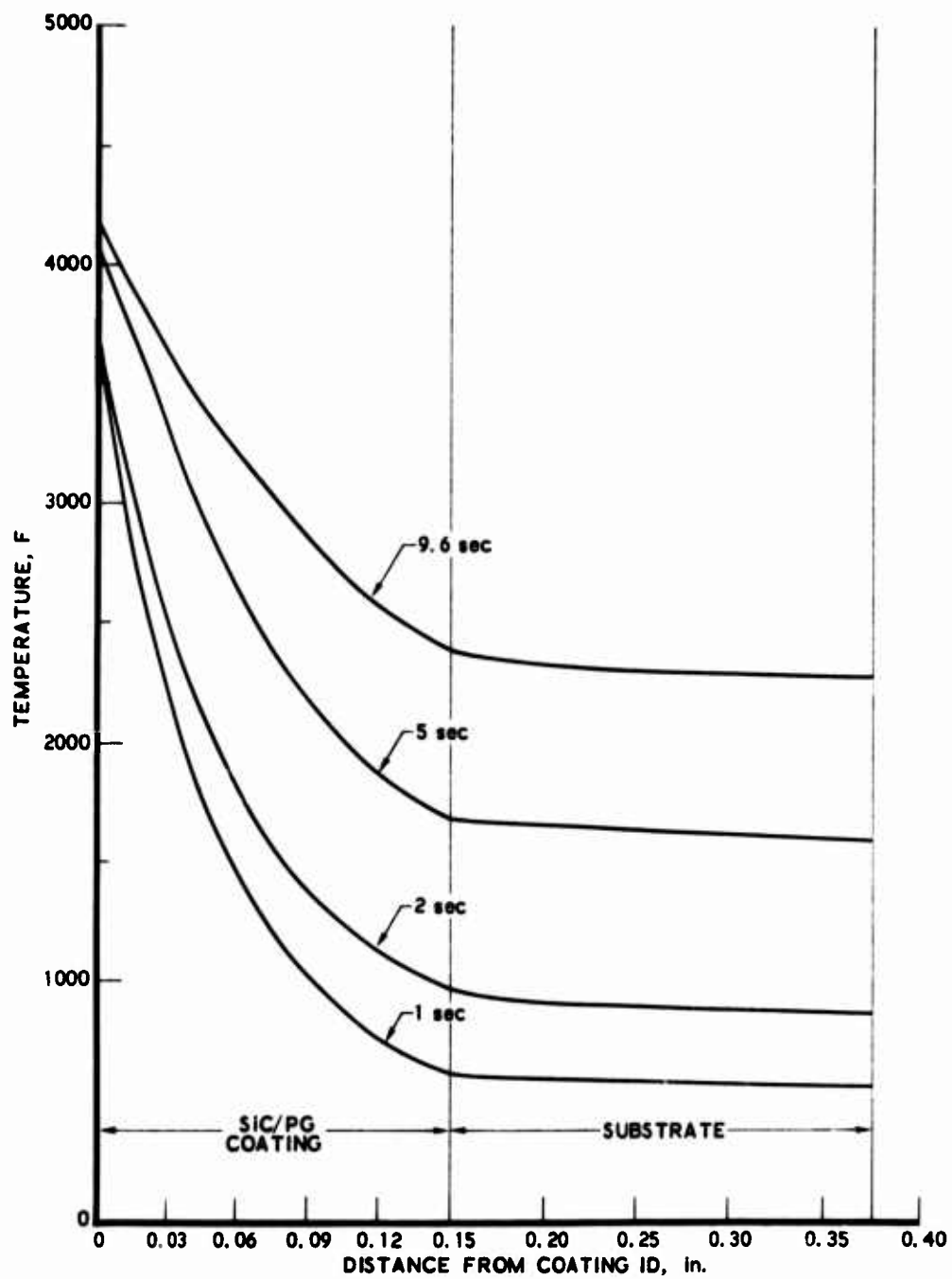Fig. 39. PG Cell Height vs Time for Various Heating Conditions

Fig. 40. Temperature Profile on C_o Specimen No. 4
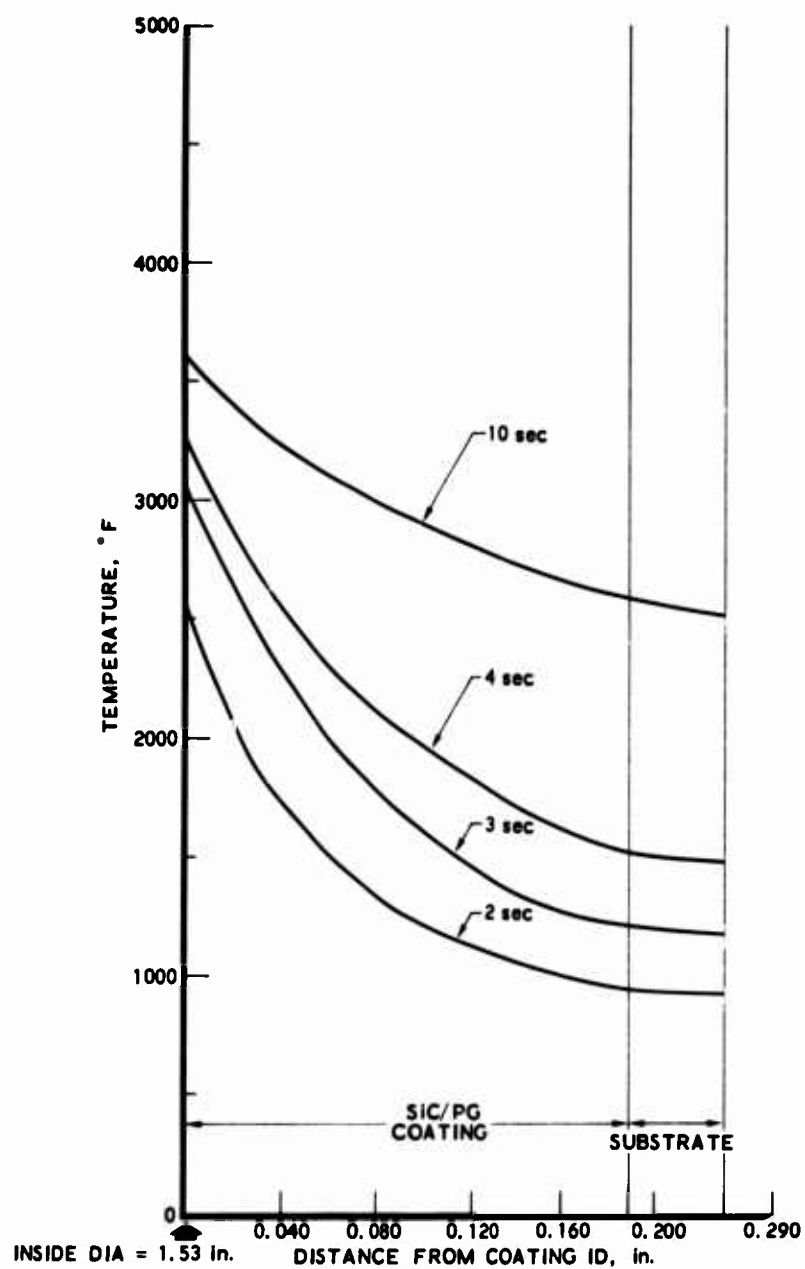
Fig. 41. Temperature Profile on C_o Specimen No. 8
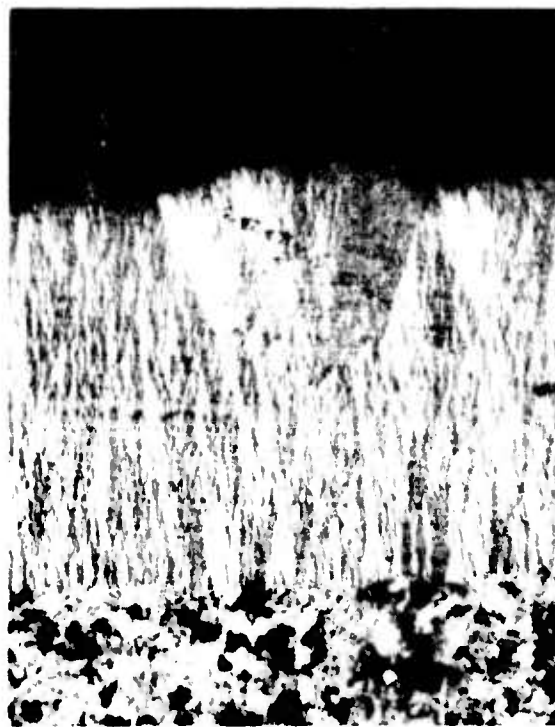
Fig. 42. MTC PG Mode Coating at Entrance (× 100)

Fig. 43. MTC PG Mode Coating at Exit (× 100)

Fig. 44. MTC PG Mode Coating at Exit
Showing Structure Anomaly
(× 1000)

III. CONCLUSIONS AND RECOMMENDATIONS

The conclusions and recommendations that have been derived from the laboratory efforts accomplished during this reporting period are presented in the paragraphs that follow.

A. **CONCLUSIONS**

1. The technique for measuring circumferential and axial residual strains in axisymmetrical bodies of revolution that were employed for this program is shown to be a method that is both cost effective and reliable for experimentally determining the maximum net inside diameter stresses of various coatings. Furthermore, this technique allows separation of the substrate-induced, or shrink-fit, stresses from the inherent coating stresses. The resultant stresses for both the PG/AGSR and the SiC-PG/ATJ inserts are of a magnitude and direction that are comparable to those predicted analytically. The sophistication of this technique is more than adequate for the level of confidence required for the variety of properties inputed to the stress solution.

2. The residual stress experiment can be a useful tool for (a) verifying new analyses as they are developed, and (b) experimentally verifying the stress levels that are a result of variations in processing parameters.

3. Stresses in the 13-in. inside diameter ARC PG on the AGSR insert are opposite in direction to the stresses in the 12-1/2-in. inside diameter ARC SiC-PG/ATJ insert.

4. The inherent circumferential coating stresses in both the aforementioned materials are greater than the axial stresses. They are opposite in direction to the substrate-induced stresses and to the net stresses, the substrate shrink stress being of the greater magnitude in all cases and locations.

5. The maximum net residual stress in the 13-in. inside diameter ARC PG on the AGSR insert is on the order of 5000 psi (utilizing SoRI property data) and compressive at the exit plane of the insert.

6. The maximum net stress in the 12-1/2-in. inside diameter ARC codeposited SiC-PG on the ATJ insert is less than 2000 psi in tension.

7. The inherent stresses within the ARC PG coating are beneficial to the overall insert stress state.

Preceding page blank

8. The ARC PG has the highest a-b plane CTE and lowest c axis CTE of those measured. The UK PG exhibited the opposite trend in thermal expansion, which is characteristic of its substrate nucleated deposition. The ratio of $\alpha c/\alpha ab$ for the UK was 18:1 between 0 and 2000°F compared with a value of 10:1 for the ARC material.

9. An examination of the thermal expansion characteristics of carbon-carbon structures that were developed for reentry application indicate that the carbon-carbon family of materials can be tailored to produce a material with a $\Delta l/l_o$ curve which matches that of PG in the hoop or circumferential direction up to the deposition temperature of PG.

10. The behavior of PG coatings above the deposition temperature (i.e., lattice reorientation) is not well defined.

11. The two TRW thermal stress samples examined by Aerospace were of insufficient duration to induce in-depth microstructure changes within the coating.

12. Processing parameters can be varied within a deposition run to tailor the end structure of a PG coating.

13. A possible technique for driving the inside diameter compressive stresses of the PG coating toward 0 (or slightly tensile) may be to deposit a more anisotropic material on a lower CTE carbon-carbon substrate; the goal being to increase primary inside diameter tensile loading of the coating while maintaining or reducing the shrink-fit stress.

B. RECOMMENDATIONS

1. It is recommended that the residual stresses of a 7-in. inside diameter UK PG coated nozzle be experimentally determined and compared with those of the 7-in. ARC PG coated nozzle. (The latter insert was run too late to be included in this report and will be presented in the year-end report.)

2. It is further recommended that the above experimental procedure be used to verify the effects of coating processing variables or of substrate variations, or both, on the stress state of small (1- to 3-in. inside diameter), right circular cylinder samples. By doing this, the experiment can be a useful tool in (a) verifying the analysis, and (b) empirically evaluating the effects of process variables.

3. The effects of heat treatment on coating stability should be examined. There is an existing ARC 7-in. PG insert that may be applicable for this effort. The ability to totally remove the AGSR without coating degradation has been demonstrated on another 7-in. ARC PG insert that was evaluated subsequent to this reporting period.

4. The experimental procedure for residual stress measurements
    should be modified to utilize an existing tracer lathe so that a
    constant substrate can be maintained when evaluating nozzle
    shapes.

5. The in-depth unit C_0 of PG coated inserts that have been subjected
    to long-duration (>60 seconds), high-temperature (>6000°F)
    firings should be evaluated.

REFERENCES

1. W. W. Lozier and M. B. Manofsy, "Properties and Performance of Pyrolytic Graphite." Paper presented at the Research Conference on the Mechanical Properties of Engineering Ceramics. North Carolina State College, Raleigh, N. C. 9-11 March 1960.

2. *Initial Progress Report*, Contract No. 18-2580, High Temperature Materials, Inc., Boston, Mass. (31 May 1961).

3. *Research Summary for Period 1 June 1960 to 1 August 1960*, No. 36-4, Vol. II, Jet Propulsion Laboratory, California Institute of Technology, Pasadena, California, pp. 20-23 (1 September 1960).

4. E. R. Stover, *Effects of Annealing on the Structure of Pyrolytic Graphite*, Report No. 60-RL-2564 M, General Electric Research Laboratory, Schenectady, N. Y. (November 1960).

5. W. H. Smith and D. H. Leeds, "Pyrolytic Graphite." *Modern Materials*, Vol. 7 (1970).

Preceding page blank

LABORATORY OPERATIONS

The Laboratory Operations of The Aerospace Corporation is conducting experimental and theoretical investigations necessary for the evaluation and application of scientific advances to new military concepts and systems. Versatility and flexibility have been developed to a high degree by the laboratory personnel in dealing with the many problems encountered in the nation's rapidly developing space and missile systems. Expertise in the latest scientific developments is vital to the accomplishment of tasks related to these problems. The laboratories that contribute to this research are:

Aerophysics Laboratory: Launch and reentry aerodynamics, heat transfer, reentry physics, chemical kinetics, structural mechanics, flight dynamics, atmospheric pollution, and high-power gas lasers.

Chemistry and Physics Laboratory: Atmospheric reactions and atmospheric optics, chemical reactions in polluted atmospheres, chemical reactions of excited species in rocket plumes, chemical thermodynamics, plasma and laser-induced reactions, laser chemistry, propulsion chemistry, space vacuum and radiation effects on materials, lubrication and surface phenomena, photosensitive materials and sensors, high precision laser ranging, and the application of physics and chemistry to problems of law enforcement and biomedicine.

Electronics Research Laboratory: Electromagnetic theory, devices, and propagation phenomena, including plasma electromagnetics; quantum electronics, lasers, and electro-optics; communication sciences, applied electronics, semiconducting, superconducting, and crystal device physics, optical and acoustical imaging; atmospheric pollution; millimeter wave and far-infrared technology.

Materials Sciences Laboratory: Development of new materials; metal matrix composites and new forms of carbon; test and evaluation of graphite and ceramics in reentry; spacecraft materials and electronic components in nuclear weapons environment; application of fracture mechanics to stress corrosion and fatigue-induced fractures in structural metals.

Space Physics Laboratory: Atmospheric and ionospheric physics, radiation from the atmosphere, density and composition of the atmosphere, aurorae and airglow; magnetospheric physics, cosmic rays, generation and propagation of plasma waves in the magnetosphere; solar physics, studies of solar magnetic fields; space astronomy, x-ray astronomy; the effects of nuclear explosions, magnetic storms, and solar activity on the earth's atmosphere, ionosphere, and magnetosphere; the effects of optical, electromagnetic, and particulate radiations in space on space systems.

THE AEROSPACE CORPORATION
El Segundo, California